arXiv:1302.4282v2 [hep-ph] 25 Apr 2013

Heavy Quarkonium Production through the Semi-Exclusive e^+e^- Annihilation Channels around the Z^0 Peak

Zhan Sun, Xing-Gang Wu,[*] Gu Chen, Jun Jiang, and Zhi Yang
Department of Physics, Chongqing University, Chongqing 401331, P.R. China

(Dated: April 26, 2013)

Within the framework of the non-relativistic QCD, we make a detailed discussion on the heavy quarkonium production at a e^+e^- collider with high luminosity up to $\mathcal{L} \propto 10^{34-36}\mathrm{cm}^{-2}\mathrm{s}^{-1}$ and with the collision energy around the Z^0 peak. They are produced through the semi-exclusive channels $e^+e^- \to |H_{Q\bar{Q}}\rangle + X$ with $X = Q\bar{Q}$ or gg. Here the heavy quark $Q = b$ or c respectively. It is noted that in addition to the color-singlet $1S$-level quarkonium states, the color-singlet quarkonium states at the $2S$-level and the $1P$-level, and the color-octet quarkonium state $|(Q\bar{Q})[1^3S_1^{(\mathbf{8})}]g\rangle$ can also provide sizable contributions. The heavy quarkonium transverse momentum and rapidity distributions for the e^+e^- collision energy $E_{cm} = m_Z$ are presented. For the charmonium or bottomonium production via the Z^0 propagator, there is approximate "spin degeneracy" for the spin-triplet and spin-singlet quarkonium states. Furthermore, uncertainties for the total cross sections are predicted by taking $m_c = 1.50 \pm 0.15$ GeV and $m_b = 4.90 \pm 0.15$ GeV. Around $E_{cm} = m_Z$, due to the Z^0-boson resonance effect, total cross sections for the channels via the Z^0-propagator become much larger than the channels via the photon propagator. Then, in addition to the B factories as BABAR and Belle and the hadronic colliders as Tevatron and LHC, such a super Z-factory will provide an excellent platform for studying the heavy quarkonium properties.

PACS numbers: 13.66.Bc, 12.38.Bx, 12.39.Jh

I. INTRODUCTION

The investigation of the heavy quarkonium, e.g. charmonium and bottomonium, is helpful for us to achieve a deeper understanding of QCD in both the perturbative and nonperturbative sectors [1–11]. A comprehensive review of heavy quarkonium physics can be found in Ref.[12]. In comparison to the hadronic colliders as Tevatron and LHC, an e^+e^--collider has many advantages, such as it provides a cleaner environment and the collision energy of the incoming electron-positron beams is well under control. Recently, a super Z factory running at an energy around the Z^0-boson mass with a high luminosity $\mathcal{L} \simeq 10^{34-36}\mathrm{cm}^{-2}\mathrm{s}^{-1}$, similar to the GigaZ program of the Internal Linear Collider [13, 14], has been suggested [15]. In the present paper, we will concentrate our attention on the heavy quarkonium production at such a super Z factory. This can be a useful reference for experimental studies and also be a useful compensation for the present BABAR and Belle results on the heavy quarkoniums.

Within the framework of non-relativistic quantum chromodynamics (NRQCD) [16], the production process can be factorized into a sum of products of the short-distance coefficients and the NRQCD long-distance matrix elements. The short-distance coefficients are perturbatively calculable in a power series of α_s at the energy scale around the heavy quark mass, which can be determined by matching the results obtained under full QCD and NRQCD accordingly. Generally, the non-perturbative long-distance matrix elements can be determined from lattice QCD calculations, or by fitting the prediction with the experimental data, or be roughly estimated by means of NRQCD velocity power counting rule. It has been shown that the matching of the color-octet matrix elements from the hadronic experiments strongly depends on the parton distribution function (PDF) [17–21], and the PDF uncertainty usually provides one of the key errors for theoretical estimation. Regarding to this point, the e^+e^- collider provides a better platform for precise studies than the hadronic colliders.

Within the framework of NRQCD, the physical state of a heavy quarkonium is generally regarded as a superposition of Fock states, and the relative importance among those infinite ingredients is evaluated by the velocity scaling rule [16]. When the $(Q\bar{Q})$-pair in the hadron $|H_{Q\bar{Q}}\rangle$ is in color-singlet state, it usually gives the dominant contribution to the heavy quarkonium productions and decays; while the color-octet $(Q\bar{Q})$-pair is usually powers of v suppressed. Here v stands for the typical velocity of the heavy quark and anti-quark in the quarkoniom rest frame, $v^2 \simeq 0.23$ for $(c\bar{c})$-quarkonium and $v^2 \simeq 0.08$ for $(b\bar{b})$-quarkonium. For example, in the velocity expansion, we have

$$|h_Q\rangle = \mathcal{O}(1)|Q\bar{Q}[^1P_1^{(\mathbf{1})}]\rangle + \mathcal{O}(v)|Q\bar{Q}[^1S_0^{(\mathbf{8})}]g\rangle + \cdots \quad (1)$$

$$|\chi_{QJ}\rangle = \mathcal{O}(1)|Q\bar{Q}[^3P_J^{(\mathbf{1})}]\rangle + \mathcal{O}(v)|Q\bar{Q}[^3S_1^{(\mathbf{8})}]g\rangle + \cdots \quad (2)$$

where $Q = b$ or c. Throughout the paper, we denote the $(Q\bar{Q})$-quarkonium with an extra superscript $(\mathbf{8})$ to stand for the color-octet state and the superscript $(\mathbf{1})$ to stand for the color-singlet state. Later on, without introducing any confusion, we omit the superscript $(\mathbf{1})$ for the color-singlet state. The angular momentum of

---

[*] Electronic address: wuxg@cqu.edu.cn

the quarkonium is set in the square brackets. The color-octet $(Q\bar{Q})$-pair can give sizable and observable contributions in certain cases or in certain kinematic regions when the color-singlet terms are highly suppressed by the hard scattering part. For example, the energy spectrum of the charged lepton for the color-octet components of the B_c meson is dominant over its color-singlet component when the lepton has high energy [22].

In the present paper, we will make a detailed discussion on the heavy quarkonium production at the super Z factory via the following two semi-exclusive channels: $e^+e^- \to \gamma^*/Z^0 \to |H_{Q\bar{Q}}\rangle + Q\bar{Q}$ and $e^+e^- \to \gamma^*/Z^0 \to |H_{Q\bar{Q}}\rangle + gg$. At the present, these two processes, together with the present BABAR and Belle data, are widely adopted for estimating the color-octet components. However, the present estimations of them (especially for the charmonium case) are inconsistent with each other, c.f. Refs.[23–25]. Thus, it would be helpful to find a new platform, such as the super Z factory, to learn more of its properties. More explicitly, we will deal with the following production processes:

$$
\begin{aligned}
& e^+e^- \to Z^0, \gamma^* \to |(Q\bar{Q})[(1^3S_1)\,, (2^3S_1)\,, (1^1S_0)\,, (2^1S_0)]\rangle + Q\bar{Q}, \\
& e^+e^- \to Z^0, \gamma^* \to |(Q\bar{Q})[(1^1P_1)\,, (1^3P_0)\,, (1^3P_1)\,, (1^3P_2)]\rangle + Q\bar{Q}, \\
& e^+e^- \to Z^0 \to |(Q\bar{Q})[\left(1^1S_0^{(\mathbf{8})}\right), \left(1^3S_1^{(\mathbf{8})}\right)]g\rangle + Q\bar{Q} \to \psi_Q + Q\bar{Q} \\
& e^+e^- \to Z^0 \to |(Q\bar{Q})[\left(1^1S_0^{(\mathbf{8})}\right)]g\rangle + Q\bar{Q} \to h_Q + Q\bar{Q} \\
& e^+e^- \to Z^0 \to |(Q\bar{Q})[\left(1^3S_1^{(\mathbf{8})}\right)]g\rangle + Q\bar{Q} \to \chi_{QJ} + Q\bar{Q}
\end{aligned}
$$

and

$$
\begin{aligned}
& e^+e^- \to Z^0, \gamma^* \to |(Q\bar{Q})[(1^3S_1)\,, (2^3S_1)]\rangle + gg, \\
& e^+e^- \to Z^0 \to |(Q\bar{Q})[(1^1S_0)\,, (2^1S_0)]\rangle + gg, \\
& e^+e^- \to Z^0 \to |(Q\bar{Q})[\left(1^1S_0^{(\mathbf{8})}\right), \left(1^3S_1^{(\mathbf{8})}\right)]g\rangle + g \to \psi_Q + g \\
& e^+e^- \to Z^0 \to |(Q\bar{Q})[\left(1^1S_0^{(\mathbf{8})}\right)]g\rangle + g \to h_Q + g \\
& e^+e^- \to Z^0 \to |(Q\bar{Q})[\left(1^3S_1^{(\mathbf{8})}\right)]g\rangle + g \to \chi_{QJ} + g
\end{aligned}
$$

where the heavy quark $Q = c$ or b respectively. It is noted that due to the absence of Fig.(4c) (by Furry Theorem) for the ψ_Q production from the channel $e^+e^- \to Z^0 \to \psi_Q + Q\bar{Q}$, the contribution of the component $|(Q\bar{Q})[\left(1^3P_J^{(\mathbf{8})}\right)]g\rangle$ is negligible. In this paper, we will only focus on the dominant color-octet channels listed above [1].

Principally, there are two approaches to deal with the heavy meson hadroproduction. One is the fragmentation approach, which automatically sums up the dominant contributions, including some important higher-order effects, into the total/differential cross sections by using the Dokshitzer-Gribov-Lipatov-Altarelli-Parisi evolution equation. The fragmentation approach is comparatively simple and can reach to leading logarithm order or even higher orders more easily, but is satisfied only in the cases if one is only interested in the produced meson itself. The other one is the so-called complete calculation approach, in which we directly deal with the full hard scattering amplitude without any approximations. This approach sometimes is hard to derive the analytical expression even at the leading order, but this approach retains the information of the accompanied quark or gluon jets and is experimentally more useful. In the present paper, we will mainly adopt the complete pQCD calculation approach to deal with these channels.

In comparison to the B factories as BABAR and Belle, we will show that a large number of heavy quarkonium events can be generated due to the Z^0-boson resonance effect. Some interesting examples for the heavy quarkonium production at such a super Z factor can be found in Refs.[26–32]. Moreover, it is found that at the super Z factory, some novel features will appear. For example, when $(Q\bar{Q})$ is in color-singlet, the channel $e^+e^- \to Z^0 \to |H_{Q\bar{Q}}\rangle + Q\bar{Q}$ can not distinguish the spin-singlet and spin-triplet S-wave states, which can be regarded as the approximate “spin degeneracy”.

---

[1] There are other less important channels, for example, for the channel $e^+e^- \to |H_{Q\bar{Q}}\rangle + gg$, we find its total cross-section from the color-singlet P-wave quarkonium states is also negligible. We will not consider them in the present paper.

The remaining part of the paper is organized as follows. In Sec.II, we present the calculation technique for dealing with the heavy quarkonium production processes $e^+e^- \to |H_{Q\bar{Q}}\rangle + Q\bar{Q}$ and $e^+e^- \to |H_{Q\bar{Q}}\rangle + gg$, where the intermediate $(Q\bar{Q})$-state is in either color-singlet or color-octet state respectively. In Sec.III, we present our numerical results and discussions. Total and differential cross sections are discussed, and we adopt the fragmentation approach for a further explanation of the “spin degeneracy”. Sec.IV is reserved for a summary.

II. FORMULATION AND TECHNIQUE

According to the NRQCD framework, the differential cross section for the process, $e^+e^- \to |H_{Q\bar{Q}}\rangle + X$, can be factorized as [16, 33] :

$$d\sigma = \sum_n d\hat{\sigma}\left(e^+e^- \to (Q\bar{Q})[n] + X\right)\frac{\langle 0|\mathcal{O}^H(n)|0\rangle}{N_{col}N_{pol}}. \quad (3)$$

The production matrix element $\langle 0|\mathcal{O}^H(n)|0\rangle$ is proportional to the inclusive transition probability of the intermediate perturbative $(Q\bar{Q})$-pair in $[n]$-state into the final bound-state $|H_{Q\bar{Q}}\rangle$. The symbol $[n] = [m^{2S+1}L_J^{(\mathbf{1}),(\mathbf{8})}]$ with definite energy level m, spin S, orbital angular momentum L and total angular momentum J, represents the above mentioned states for the intermediate $(Q\bar{Q})$-pair respectively; i.e.,

$$n = 1^1S_0, 2^1S_0, 1^1P_1, 1^1S_0^{(\mathbf{8})}; 1^3S_1, 2^3S_1, 1^3P_J, 1^3S_1^{(\mathbf{8})},$$

with $J = 0, 1, 2$. These states provide the dominant contributions to the processes $e^+e^- \to \gamma^*/Z^0 \to |H_{Q\bar{Q}}\rangle + Q\bar{Q}$ and $e^+e^- \to \gamma^*/Z^0 \to |H_{Q\bar{Q}}\rangle + gg$ up to $\mathcal{O}(v^4)$. The parameters N_{col} and N_{pol} refer to the number of colors and polarization states of the intermediate $(Q\bar{Q})$-pair. $N_{col} = 1$ for the color-singlet state or $N_{col} = N_c^2 - 1$ for the color-octet state. As for the color-singlet components, their matrix elements can be directly related to the wavefunction at the origin or the first derivative of the wavefunction at the origin, which can be computed via the potential modes and/or potential NRQCD and/or lattice QCD. As for the color-octet matrix elements, they can be estimated by using the velocity scaling rule or be determined experimentally.

The short-distance cross-section $d\hat{\sigma}(e^+(p_2)e^-(p_1) \to (Q\bar{Q})[n] + X)$ can be written in the following form:

$$d\hat{\sigma}\left(e^+e^- \to (Q\bar{Q})[n] + X\right) = \frac{\overline{\sum}|\mathcal{M}|^2 d\Phi_k}{4\sqrt{(p_1\cdot p_2)^2 - m_e^4}}, \quad (4)$$

where k stands for the number of final state particles, $\overline{\sum}$ means that we need to average over the spin states of the initial particles and to sum over the spin and color of all final particles. The phase space with k final-state particles :

$$d\Phi_k = (2\pi)^4\delta^4\left(p_1 + p_2 - \sum_{f=3}^{k+2} p_f\right)\prod_{f=3}^{k+2}\frac{d^3p_f}{(2\pi)^3 2p_f^0}.$$

The phase-space integration can be done with the help of a combination of the subroutines RAMBOS [34] and VEGAS [35], which can be found in generators GENXICC [36] and BCVEGPY [37]. After generating proper phase-space points, one can calculate the numerical value for the squared amplitude $|\mathcal{M}|^2$. Furthermore, in deriving the fragmentation functions, a splitting phase space is helpful. To be useful reference, we put some details for doing the phase-space splitting in the appendix.

The hard scattering amplitude for those processes can be written as,

$$i\mathcal{M} = \mathcal{C}\, L^{\mu}_{rr'} D_{\mu\nu}\sum_i \mathcal{A}_i^{\nu}. \quad (5)$$

The leptonic current

$$L^{\mu}_{rr'} = \bar{v}_r(p_2)\Gamma^{\mu}u_{r'}(p_1). \quad (6)$$

The value of i is process dependent, e.g.

$$i = 4 \ \text{ for } \ e^+e^- \to (Q\bar{Q})[n] + Q\bar{Q}$$
$$i = 6 \ \text{ for } \ e^+e^- \to (Q\bar{Q})[n] + gg$$

for $(Q\bar{Q})[n]$ in color-singlet state; while for the case of color-octet production,

$$i = 2 \ \text{ for } \ e^+e^- \to Z^0 \to |(Q\bar{Q})[\left(1^1S_0^{(\mathbf{8})}\right)]g\rangle + g$$
$$\text{for } \ e^+e^- \to Z^0 \to |(Q\bar{Q})[\left(1^3S_1^{(\mathbf{8})}\right)]g\rangle + g$$
$$i = 6 \ \text{ for } \ e^+e^- \to Z^0 \to |(Q\bar{Q})[\left(1^1S_0^{(\mathbf{8})}\right)]g\rangle + Q\bar{Q}$$
$$i = 8 \ \text{ for } \ e^+e^- \to Z^0 \to |(Q\bar{Q})[\left(1^3S_1^{(\mathbf{8})}\right)]g\rangle + Q\bar{Q}$$

The spin-indices r and r' stand for the spin projections of the initial electron and positron. For the quarkonium production through the Z^0-boson propagator, the vertex $\Gamma^{\mu} = \gamma^{\mu}(1 - 4\sin^2\theta_w - \gamma^5)$ and the propagator $D_{\mu\nu} = \frac{i}{k^2 - m_Z^2 + im_Z\Gamma_z}\left(-g_{\mu\nu} + k_{\mu}k_{\nu}/k^2\right)$, where Γ_z stands for the total decay width of Z^0 boson. While, for the quarkonium production through the photon propagator: the vertex $\Gamma^{\mu} = \gamma^{\mu}$ and the propagator $D_{\mu\nu} = -\frac{i}{k^2}g_{\mu\nu}$.

The overall parameter $\mathcal{C} = \mathcal{C}_s$ or $\mathcal{C}_o$ for the production of the color-singlet or the color-octet quarkonium state respectively. The simplified hard scattering amplitudes $\mathcal{A}_i^{\nu}$ are process dependent, which will be presented in the following subsections.

A. Color-Singlet Case

1. $e^+(p_2)e^-(p_1) \to |H_{Q\bar{Q}}\rangle(p_3) + Q(p_4)\bar{Q}(p_5)$

Typical Feynman diagrams for the process $e^+e^- \to |H_{Q\bar{Q}}\rangle + Q\bar{Q}$ through color-singlet $(Q\bar{Q})$-quarkonium

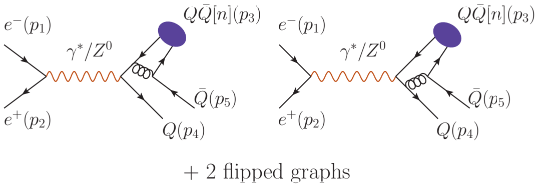

FIG. 1: Feynman diagrams for $e^+e^- \to |H_{Q\bar{Q}}\rangle + Q\bar{Q}$ via the perturbative state $(Q\bar{Q})[n]$. Here Q stands for c or b quark, and [n] stands for the color-singlet quarkonium state.

states are presented in Fig.(1). According to the Feynman diagrams, we can write down the simplified hard scattering amplitudes $\mathcal{A}_i^\nu$ of the short-distance cross-section $d\hat{\sigma}(e^+e^- \to (Q\bar{Q})[n] + Q\bar{Q})$.

For $[n]$ stands for the color-single S-wave states, we have

$$\mathcal{A}_1^\nu = \bar{u}_s(p_4)\Gamma^\nu_{Q\bar{Q}}\frac{-\not{p}_3 - \not{p}_5 + m_Q}{(p_3+p_5)^2 - m_Q^2}\gamma_\rho\frac{\Pi^{0(1)}_{(Q\bar{Q})}(p_3)}{(p_{31}+p_5)^2}\gamma_\rho v_{s'}(p_5), \tag{7}$$

$$\mathcal{A}_2^\nu = \bar{u}_s(p_4)\gamma_\rho\frac{\not{p}_4 + \not{p}_5 + \not{p}_{31} + m_Q}{(p_4+p_5+p_{31})^2 - m_Q^2}\Gamma^\nu_{Q\bar{Q}}\frac{\Pi^{0(1)}_{(Q\bar{Q})}(p_3)}{(p_{31}+p_5)^2}\gamma_\rho v_{s'}(p_5), \tag{8}$$

$$\mathcal{A}_3^\nu = \bar{u}_s(p_4)\gamma_\rho\frac{\Pi^{0(1)}_{(Q\bar{Q})}(p_3)}{(p_{32}+p_4)^2}\gamma_\rho\frac{\not{p}_3 + \not{p}_4 + m_Q}{(p_3+p_4)^2 - m_Q^2}\Gamma^\nu_{Q\bar{Q}}v_{s'}(p_5), \tag{9}$$

$$\mathcal{A}_4^\nu = \bar{u}_s(p_4)\gamma_\rho\frac{\Pi^{0(1)}_{(Q\bar{Q})}(p_3)}{(p_{32}+p_4)^2}\Gamma^\nu_{Q\bar{Q}}\frac{-\not{p}_4 - \not{p}_5 - \not{p}_{32} + m_Q}{(p_4+p_5+p_{32})^2 - m_Q^2}\gamma_\rho v_{s'}(p_5). \tag{10}$$

For $[n]$ stands for the color-singlet P-wave states, we have

$$\mathcal{A}_1^{\nu,S=0,L=1} = \bar{u}_s(p_4)\epsilon^l_\alpha(p_3)\frac{d}{dq_\alpha}\left[\Gamma^\nu_{Q\bar{Q}}\frac{-\not{p}_3 - \not{p}_5 + m_Q}{(p_3+p_5)^2 - m_Q^2}\gamma_\rho\frac{\Pi^0_{(Q\bar{Q})}(p_3)}{(p_{31}+p_5)^2}\gamma_\rho\right]_{q=0} v_{s'}(p_5), \tag{11}$$

$$\mathcal{A}_2^{\nu,S=0,L=1} = \bar{u}_s(p_4)\epsilon^l_\alpha(p_3)\frac{d}{dq_\alpha}\left[\gamma_\rho\frac{\not{p}_4 + \not{p}_5 + \not{p}_{31} + m_Q}{(p_4+p_5+p_{31})^2 - m_Q^2}\Gamma^\nu_{Q\bar{Q}}\frac{\Pi^0_{(Q\bar{Q})}(p_3)}{(p_{31}+p_5)^2}\gamma_\rho\right]_{q=0} v_{s'}(p_5), \tag{12}$$

$$\mathcal{A}_3^{\nu,S=0,L=1} = \bar{u}_s(p_4)\epsilon^l_\alpha(p_3)\frac{d}{dq_\alpha}\left[\gamma_\rho\frac{\Pi^0_{(Q\bar{Q})}(p_3)}{(p_{32}+p_4)^2}\gamma_\rho\frac{\not{p}_3 + \not{p}_4 + m_Q}{(p_3+p_4)^2 - m_Q^2}\Gamma^\nu_{Q\bar{Q}}\right]_{q=0} v_{s'}(p_5), \tag{13}$$

$$\mathcal{A}_4^{\nu,S=0,L=1} = \bar{u}_s(p_4)\epsilon^l_\alpha(p_3)\frac{d}{dq_\alpha}\left[\gamma_\rho\frac{\Pi^0_{(Q\bar{Q})}(p_3)}{(p_{32}+p_4)^2}\Gamma^\nu_{Q\bar{Q}}\frac{-\not{p}_4 - \not{p}_5 - \not{p}_{32} + m_Q}{(p_4+p_5+p_{32})^2 - m_Q^2}\gamma_\rho\right]_{q=0} v_{s'}(p_5). \tag{14}$$

and

$$\mathcal{A}_1^{\nu,S=1,L=1} = \bar{u}_s(p_4)\varepsilon^{J_z}_{\alpha\beta}(p_3)\frac{d}{dq_\alpha}\left[\Gamma^\nu_{Q\bar{Q}}\frac{-\not{p}_3 - \not{p}_5 + m_Q}{(p_3+p_5)^2 - m_Q^2}\gamma_\rho\frac{\Pi^\beta_{(Q\bar{Q})}(p_3)}{(p_{31}+p_5)^2}\gamma_\rho\right]_{q=0} v_{s'}(p_5), \tag{15}$$

$$\mathcal{A}_2^{\nu,S=1,L=1} = \bar{u}_s(p_4)\varepsilon^{J_z}_{\alpha\beta}(p_3)\frac{d}{dq_\alpha}\left[\gamma_\rho\frac{\not{p}_4 + \not{p}_5 + \not{p}_{31} + m_Q}{(p_4+p_5+p_{31})^2 - m_Q^2}\Gamma^\nu_{Q\bar{Q}}\frac{\Pi^\beta_{(Q\bar{Q})}(p_3)}{(p_{31}+p_5)^2}\gamma_\rho\right]_{q=0} v_{s'}(p_5), \tag{16}$$

$$\mathcal{A}_3^{\nu,S=1,L=1} = \bar{u}_s(p_4)\varepsilon^{J_z}_{\alpha\beta}(p_3)\frac{d}{dq_\alpha}\left[\gamma_\rho\frac{\Pi^\beta_{(Q\bar{Q})}(p_3)}{(p_{32}+p_4)^2}\gamma_\rho\frac{\not{p}_3 + \not{p}_4 + m_Q}{(p_3+p_4)^2 - m_Q^2}\Gamma^\nu_{Q\bar{Q}}\right]_{q=0} v_{s'}(p_5), \tag{17}$$

$$\mathcal{A}_4^{\nu,S=1,L=1} = \bar{u}_s(p_4)\varepsilon^{J_z}_{\alpha\beta}(p_3)\frac{d}{dq_\alpha}\left[\gamma_\rho\frac{\Pi^{\beta}_{(Q\bar{Q})}(p_3)}{(p_{32}+p_4)^2}\Gamma^{\nu}_{Q\bar{Q}}\frac{-\not{p}_4-\not{p}_5-\not{p}_{32}+m_Q}{(p_4+p_5+p_{32})^2-m_Q^2}\gamma_\rho\right]_{q=0} v_{s'}(p_5). \qquad (18)$$

The parameters s and s' stand for the spin projections of the outgoing quark and antiquark respectively.

For convenience, we have introduced a general interaction vertex

$$\Gamma^{\nu}_{Q\bar{Q}} = \gamma^{\nu}(\alpha P_L + \beta P_R), \qquad (19)$$

where $P_L = (1-\gamma^5)/2$ and $P_R = (1+\gamma^5)/2$. Here $\alpha = 2 - \frac{8}{3}\sin^2\theta_w$ and $\beta = -\frac{8}{3}\sin^2\theta_w$ for $(Zc\bar{c})$-vertex, $\alpha = 2 - \frac{4}{3}\sin^2\theta_w$ and $\beta = -\frac{4}{3}\sin^2\theta_w$ for $(Zb\bar{b})$-vertex, $\alpha = 1$ and $\beta = 1$ for $(\gamma^* Q\bar{Q})$-vertex, respectively.

The momenta of the constituent quarks are

$$p_{31} = \frac{m_Q}{M_{Q\bar{Q}}}p_3 + q \;\;\text{and}\;\; p_{32} = \frac{m_{\bar{Q}}}{M_{Q\bar{Q}}}p_3 - q, \qquad (20)$$

where $M_{Q\bar{Q}} = m_Q + m_{\bar{Q}}$ is implicitly adopted to ensure the gauge invariance of the hard scattering amplitude, q is the relative momentum between the two constituent quarks inside the quarkonium.

The covariant form of the projectors are

$$\Pi^{0}_{(Q\bar{Q})}(p_3) = \frac{-\sqrt{M_{Q\bar{Q}}}}{4m_Q m_{\bar{Q}}}(\not{p}_{32} - m_{\bar{Q}})\gamma_5(\not{p}_{31} + m_Q) \qquad (21)$$

and

$$\Pi^{1}_{(Q\bar{Q})}(p_3) = \epsilon^{s}_{\beta}(p_3)\Pi^{\beta}_{(Q\bar{Q})}(p_3) \qquad (22)$$

with

$$\Pi^{\beta}_{(Q\bar{Q})}(p_3) = \frac{-\sqrt{M_{Q\bar{Q}}}}{4m_Q m_{\bar{Q}}}(\not{p}_{32} - m_{\bar{Q}})\gamma^{\beta}(\not{p}_{31} + m_Q). \qquad (23)$$

Inserting these projectors into the amplitude, the amplitude can be squared, summed over the spin in the final state and averaged over the ones in the initial state. The selection of the proper angular momentum is done by performing proper polarization sum. We define:

$$\Pi_{\alpha\beta} \equiv -g_{\alpha\beta} + \frac{p_{3\alpha}p_{3\beta}}{M^2_{Q\bar{Q}}}. \qquad (24)$$

The sum over polarization for a spin-triplet S-wave state ($^3S_1$) or a spin-singlet P-wave state ($^1P_1$) is given by:

$$\sum_{J_z}\epsilon_\alpha\epsilon^*_{\alpha'} = \Pi_{\alpha\alpha'}, \qquad (25)$$

where $J_z = s_z$ or l_z respectively. For the spin-triplet P-wave states (^3P_J with $J = 0, 1, 2$), the sum over polarization is given by [33]

$$\varepsilon^{(0)}_{\alpha\beta}\varepsilon^{(0)*}_{\alpha'\beta'} = \frac{1}{3}\Pi_{\alpha\beta}\Pi_{\alpha'\beta'}$$

$$\sum_{J_Z}\varepsilon^{(1)}_{\alpha\beta}\varepsilon^{(1)*}_{\alpha'\beta'} = \frac{1}{2}\left[\Pi_{\alpha\alpha'}\Pi_{\beta\beta'} - \Pi_{\alpha\beta'}\Pi_{\alpha'\beta}\right]$$

$$\sum_{J_Z}\varepsilon^{(2)}_{\alpha\beta}\varepsilon^{(2)*}_{\alpha'\beta'} = \frac{1}{2}\left[\Pi_{\alpha\alpha'}\Pi_{\beta\beta'} + \Pi_{\alpha\beta'}\Pi_{\alpha'\beta}\right] - \frac{1}{3}\Pi_{\alpha\beta}\Pi_{\alpha'\beta'}$$

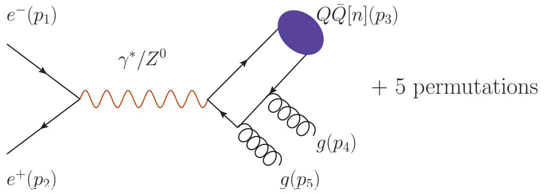

FIG. 2: Typical Feynman diagrams for $e^+e^- \to |H_{Q\bar{Q}}\rangle + gg$ through the perturbative state $(Q\bar{Q})[n]$, here Q stands for the c or b quark and [n] represents the color-singlet quarkonium states.

For the overall color-singlet parameter, we have $\mathcal{C}_s = \frac{4}{3\sqrt{3}}\frac{e^2 g_s^2}{\sin^2\theta_w\cdot(4\cos\theta_w)^2}\delta_{ij}$ for the quarkonium production through Z^0-boson propagator and $\mathcal{C}_s = \frac{4}{3\sqrt{3}}e_Q e^2 g_s^2\delta_{ij}$ for the quarkonium production through photon propagator, where e_Q stands for the electric charge of Q in unit e.

2. $e^+(p_2)e^-(p_1) \to |H_{Q\bar{Q}}\rangle(p_3) + g(p_4)g(p_5)$

Typical Feynman diagrams for the process $e^+e^- \to |H_{Q\bar{Q}}\rangle + gg$ are presented in Fig.(2). According to the Feynman diagrams, one can write down the simplified hard scattering amplitudes $\mathcal{A}_i^{\nu}$ for the short-distance cross-section $d\hat{\sigma}(e^+e^- \to (Q\bar{Q})[n] + gg)$ as

$$\mathcal{A}_1^{\nu} \;=\; \mathrm{Tr}\left[\left(\Pi^{0(1)}_{(Q\bar{Q})}(p_3)\right)\Gamma^{\nu}_{Q\bar{Q}}\frac{-\not{p}_{32}-\not{p}_4-\not{p}_5+m_Q}{(p_{32}+p_4+p_5)^2-m_Q^2}\not{\epsilon}(p_5)\frac{-\not{p}_{32}-\not{p}_4+m_Q}{(p_{32}+p_4)^2-m_Q^2}\not{\epsilon}(p_4)\right], \qquad (26)$$

and the amplitudes $\mathcal{A}_2^\nu$, $\cdots$, $\mathcal{A}_6^\nu$ can be derived by permutations.

For the overall color-singlet parameter, we have $\mathcal{C}_s = \frac{1}{2\sqrt{3}}\frac{e^2 g_s^2}{\sin^2\theta_w\cdot(4\cos\theta_w)^2}\delta_{ab}$ for the quarkonium production through Z^0-boson propagator and $\mathcal{C}_s = \frac{1}{2\sqrt{3}} e_Q e^2 g_s^2 \delta_{ab}$ for the quarkonium production through photon propagator, where $a, b = (1, \cdots, 8)$ are color indices of the two outgoing gluons.

The simplified amplitudes for the case of color-singlet P-wave states can be written down in a similar way as the process $e^+e^- \to |H_{Q\bar{Q}}\rangle + Q\bar{Q}$. Numerically, it is found that the total cross-sections for the color-singlet P-wave states are negligible, so we do not present them here.

B. Color-Octet Case

1. $e^+(p_2)e^-(p_1) \to Z^0 \to |(Q\bar{Q})[\left(1^1S_0^{(\mathbf{8})}\right), \left(1^3S_1^{(\mathbf{8})}\right)]g\rangle(p_3) + Q(p_4)\bar{Q}(p_5)$

Typical Feynman diagrams for the processes $e^+e^- \to Z^0 \to |(Q\bar{Q})[\left(1^1S_0^{(\mathbf{8})}\right)]g\rangle + Q\bar{Q}$ and $e^+e^- \to Z^0 \to |(Q\bar{Q})[\left(1^3S_1^{(\mathbf{8})}\right)]g\rangle + Q\bar{Q}$ are presented in Figs.(3,4) accordingly. It is found that

- Four Feynman diagrams as shown in both Fig.(3a) and Fig.(4a) have the same topologies as those of Fig.(1). Their simplified amplitudes $\mathcal{A}_1^\nu, \cdots, \mathcal{A}_4^\nu$ are the same as those of Eqs.(7,8,9,10). While, the overall parameter $\mathcal{C}_s$ there should be replaced by the present case of $\mathcal{C}_o$, and the color-singlet matrix element should be replaced by the color-octet matrix element.

- The two Feynman diagrams as shown in Fig.(3b) and Fig.(4b) have the same topologies, and their simplified amplitudes $\mathcal{A}_5^\nu$ and $\mathcal{A}_6^\nu$ are the same. More explicitly, we have:

$$\mathcal{A}_5^\nu = \bar{u}_s(p_4)\gamma_\rho \mathrm{Tr}\left[\gamma_\rho \frac{\Pi^{0(1)}_{(Q\bar{Q})}(p_3)}{(p_4+p_5)^2}\Gamma^\nu_{Q\bar{Q}}\frac{-\not{p}_{32}-\not{p}_4-\not{p}_5+m_Q}{(p_{32}+p_4+p_5)^2-m_Q^2}\right]v_{s'}(p_5), \tag{27}$$

$$\mathcal{A}_6^\nu = \bar{u}_s(p_4)\gamma_\rho \mathrm{Tr}\left[\gamma_\rho \frac{\not{p}_{31}+\not{p}_4+\not{p}_5+m_Q}{(p_{31}+p_4+p_5)^2-m_Q^2}\Gamma^\nu_{Q\bar{Q}}\frac{\Pi^{0(1)}_{(Q\bar{Q})}(p_3)}{(p_4+p_5)^2}\right]v_{s'}(p_5). \tag{28}$$

- The remaining two simplified amplitudes $\mathcal{A}_7^\nu$ and $\mathcal{A}_8^\nu$ for the case of $|(Q\bar{Q})[\left(1^3S_1^{(\mathbf{8})}\right)]g\rangle$ production, as shown in Fig.(4c), are

$$\mathcal{A}_7^\nu = \bar{u}_s(p_4)\Gamma^\nu_{Q\bar{Q}}\frac{-\not{p}_3-\not{p}_5+m_Q}{(p_3+p_5)^2-m_Q^2}\gamma_\rho \mathrm{Tr}\left[\frac{\Pi^1_{(Q\bar{Q})}(p_3)}{p_3^2}\gamma_\rho\right]v_{s'}(p_5), \tag{29}$$

$$\mathcal{A}_8^\nu = \bar{u}_s(p_4)\gamma_\rho \mathrm{Tr}\left[\frac{\Pi^1_{(Q\bar{Q})}(p_3)}{p_3^2}\gamma_\rho\right]\frac{\not{p}_3+\not{p}_4+m_Q}{(p_3+p_4)^2-m_Q^2}\Gamma^\nu_{Q\bar{Q}}v_{s'}(p_5). \tag{30}$$

For the overall color-octet parameters, we have $\mathcal{C}_o = \frac{e^2 g_s^2}{\sin^2\theta_w(4\cos\theta_w)^2}\times\left(\mathcal{C}_{ij}^{(a)}, \mathcal{C}_{ij}^{(b)}, \mathcal{C}_{ij}^{(c)}\right)$ respectively. Here, the color factors $\mathcal{C}_{ij}^{(a),(b),(c)}$, according to Figs.(4a,4b,4c), are:

$$\mathcal{C}_{ij}^{(a)} = \sum_{m,n}(T^a)_{in}\times(\sqrt{2}T^d)_{nm}\times(T^a)_{mj} \tag{31}$$

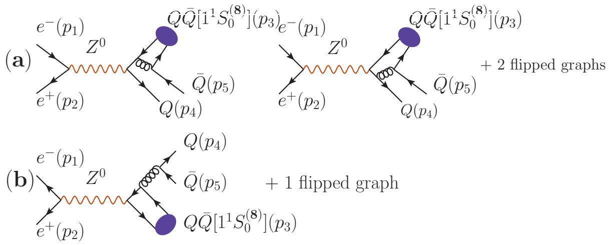

FIG. 3: Typical Feynman diagrams for $e^+e^- \to Z^0 \to |(Q\bar{Q})[\left(1^1S_0^{(\mathbf{8})}\right)]g\rangle + Q\bar{Q}$, where Q stands for c or b quark.

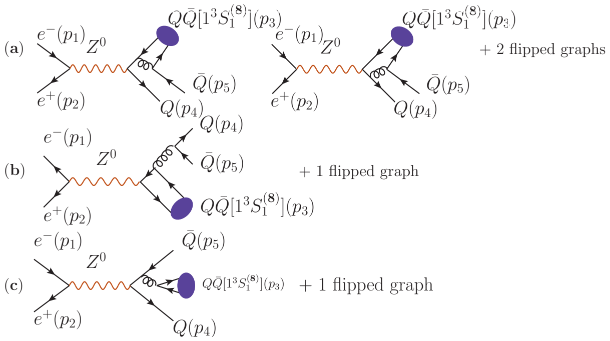

FIG. 4: Typical Feynman diagrams for $e^+e^- \to Z^0 \to |(Q\bar{Q})[\left(1^3S_1^{(\mathbf{8})}\right)]g\rangle + Q\bar{Q}$, where Q stands for c or b quark.

$$\mathcal{C}_{ij}^{(b)} = \sum_{m,n} (T^a)_{ij} \times (T^a)_{mn} \times (\sqrt{2}T^d)_{nm} \tag{32}$$

$$\mathcal{C}_{ij}^{(c)} = \sum_{m,n} (T^a)_{ij} \times (T^a)_{mn} \times (\sqrt{2}T^d)_{nm} \tag{33}$$

where $i, j, m, n = (1, 2, 3)$ are color indices of the outgoing anti-quark $\bar{Q}$, quark Q and the two constituent quarks Q and $\bar{Q}$ in the heavy quarkonium, respectively. The superscript indices (a), (b) and (c) of $\mathcal{C}_{ij}$ refer to the corresponding figures in Figs.(3,4). After simplification, we obtain

$$\mathcal{C}_{ij}^{(a)} = -\frac{\sqrt{2}}{6}T_{ij}^d,\ \mathcal{C}_{ij}^{(b)} = \mathcal{C}_{ij}^{(c)} = \frac{\sqrt{2}}{2}T_{ij}^d.$$

Here $d = (1, \cdots, 8)$ represents the color of the color-octet quarkonium.

2. $e^+(p_2)e^-(p_1) \to Z^0 \to |(Q\bar{Q})[\left(1^1S_0^{(\mathbf{8})}\right), \left(1^3S_1^{(\mathbf{8})}\right)]g\rangle(p_3) + g(p_4)$

Typical Feynman diagrams for the processes $e^+e^- \to Z^0 \to |(Q\bar{Q})[\left(1^1S_0^{(\mathbf{8})}\right), \left(1^3S_1^{(\mathbf{8})}\right)]g\rangle + g$ are presented in Fig.(5). Its first simplified amplitude $\mathcal{A}_1^\nu$ takes the form

$$\mathcal{A}_1^\nu = \mathrm{Tr}\left[\left(\Pi^{0(1)}_{(Q\bar{Q})}(p_3)\right)\Gamma^\nu_{Q\bar{Q}}\frac{-\not{p}_{32} - \not{p}_4 + m_Q}{(p_{32}+p_4)^2 - m_Q^2}\not{\epsilon}(p_4)\right], \tag{34}$$

and the second amplitude $\mathcal{A}_2^\nu$ can be obtained from $\mathcal{A}_1^\nu$ by permutation.

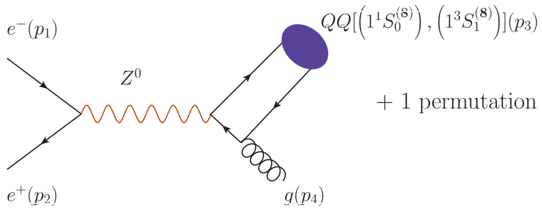
$e^-(p_1)$
Z^0
$QQ[\left(1^1S_0^{(8)}\right), \left(1^3S_1^{(8)}\right)](p_3)$
+ 1 permutation
$e^+(p_2)$
$g(p_4)$

FIG. 5: Typical Feynman diagrams for $e^+e^- \to Z^0 \to |(Q\bar{Q})[\left(1^1S_0^{(\mathbf{8})}\right), \left(1^3S_1^{(\mathbf{8})}\right)]g\rangle + g$, where Q stands for the heavy c or b quark.

For the overall color-octet parameter, we have $\mathcal{C}_o = \frac{\sqrt{2}}{2}\frac{e^2 g_s}{\sin^2\theta_w(4\cos\theta_w)^2} \times \delta_{ad}$. Here $a, d = (1, \cdots, 8)$ represent the color indices of the outgoing gluon and the color octet quarkonium, respectively.

III. NUMERICAL RESULTS

Matrix element		$\lvert\Psi(0)\rvert^2$or$\lvert\Psi'(0)\rvert^2$
$\langle 0\lvert\mathcal{O}_1^{J/\psi}(^3S_1)\rvert 0\rangle$	1.2 GeV^3	0.067 GeV^3
$\langle 0\lvert\mathcal{O}_1^{\psi'}(^3S_1)\rvert 0\rangle$	7.6×10^{-1} GeV^3	0.042 GeV^3
$\langle 0\lvert\mathcal{O}_1^{\Upsilon}(^3S_1)\rvert 0\rangle$	9.3 GeV^3	0.517 GeV^3
$\langle 0\lvert\mathcal{O}_1^{\Upsilon'}(^3S_1)\rvert 0\rangle$	4.6 GeV^3	0.256 GeV^3
$\langle 0\lvert\mathcal{O}_1^{\chi_{c1}}(^3P_1)\rvert 0\rangle$	3.2×10^{-1} GeV^5	0.018 GeV^5
$\langle 0\lvert\mathcal{O}_1^{\chi_{b1}}(^3P_1)\rvert 0\rangle$	6.1 GeV^5	0.339 GeV^5
$\langle 0\lvert\mathcal{O}_8^{J/\psi}(^3S_1)\rvert 0\rangle$	1.2×10^{-2} GeV^3	$\sim$
$\langle 0\lvert\mathcal{O}_8^{\Upsilon}(^3S_1)\rvert 0\rangle$	9.5×10^{-3} GeV^3	$\sim$
$\langle 0\lvert\mathcal{O}_8^{\chi_{c1}}(^3S_1)\rvert 0\rangle$	1.6×10^{-2} GeV^3	$\sim$
$\langle 0\lvert\mathcal{O}_8^{\chi_{b1}}(^3S_1)\rvert 0\rangle$	4.3×10^{-2} GeV^3	$\sim$

TABLE I: Input color-singlet and color-octet matrix elements [38], where the color-singlet matrix elements are related to the wavefunctions at the origin or the first derivative of the wavefunctions at the origin respectively.

In doing numerical calculation, the heavy quark masses are taken as: $m_c = 1.50^{+0.15}_{-0.15}$ GeV and $m_b = 4.90^{+0.15}_{-0.15}$ GeV. The color-singlet and color-octet non-perturbative matrix elements are taken from Ref.[38], which are presented in Table I. As for the production matrix elements, we adopt the relation

$$\langle 0|\mathcal{O}^H_{[\mathbf{1},\mathbf{8}]}(^3S_1)|0\rangle \simeq 3\langle 0|\mathcal{O}^H_{[\mathbf{1},\mathbf{8}]}(^1S_0)|0\rangle.$$

The production color-singlet matrix elements and the wavefunctions at the origin are related by [16, 33]:

$$\frac{\langle 0|\mathcal{O}_{\mathbf{1}}^{\eta_c}|0\rangle}{2N_c} \simeq \frac{\langle 0|\mathcal{O}_{\mathbf{1}}^{J/\psi}|0\rangle}{6N_c} = |\Psi_{1S}(0)|^2, \tag{35}$$

$$\frac{\langle 0|\mathcal{O}_{\mathbf{1}}^{\eta_c'}|0\rangle}{2N_c} \simeq \frac{\langle 0|\mathcal{O}_{\mathbf{1}}^{\psi'}|0\rangle}{6N_c} = |\Psi_{2S}(0)|^2 \tag{36}$$

and

$$\frac{\langle 0|\mathcal{O}_{\mathbf{1}}^{\chi_{c0}}|0\rangle}{2N_c} \simeq \frac{\langle 0|\mathcal{O}_{\mathbf{1}}^{\chi_{c1}}|0\rangle}{6N_c} \simeq \frac{\langle 0|\mathcal{O}_{\mathbf{1}}^{\chi_{c2}}|0\rangle}{10N_c} = |\Psi'_{1P}(0)|^2. \tag{37}$$

As for the production color-octet matrix elements, we adopt the relation [16]

$$\begin{aligned} \langle 0|\mathcal{O}_{\mathbf{8}}^{\chi_{c2}}(^3S_1)|0\rangle &= \frac{5}{3}\langle 0|\mathcal{O}_{\mathbf{8}}^{h_c}(^1S_0)|0\rangle \\ \langle 0|\mathcal{O}_{\mathbf{8}}^{\chi_{c1}}(^3S_1)|0\rangle &= \frac{3}{3}\langle 0|\mathcal{O}_{\mathbf{8}}^{h_c}(^1S_0)|0\rangle \\ \langle 0|\mathcal{O}_{\mathbf{8}}^{\chi_{c0}}(^3S_1)|0\rangle &= \frac{1}{3}\langle 0|\mathcal{O}_{\mathbf{8}}^{h_c}(^1S_0)|0\rangle \end{aligned} \tag{38}$$

Here the heavy-quark spin symmetry [16] has been implicitly adopted. That is, we will not distinguish the wavefunctions at the origin for the spin-singlet ($^1S_0$) state and the spin-triplet ($^3S_1$) state at the same energy level. For the bottomonium production color-singlet and color-octet matrix elements they have the similar relations as those of the charmonium.

As for the renormalization scale, we take it to be $2m_c$ for charmonium production, and $2m_b$ for bottomonium production. Other input parameters are taken from the Particle Data Group [39]: $\Gamma_Z = 2.4952$ GeV, $m_Z = 91.1876$ GeV, $\sin^2\theta_w$=0.2312. By using leading-order α_s running and $\alpha_s(mz) = 0.1184$, we obtain $\alpha_s(2m_c) = 0.237$ and $\alpha_s(2m_b) = 0.175$.

A. Properties of the color-singlet processes

The color-singlet components provide the dominant contributions to the heavy quarkonium production processes. We will make a detailed discussion on the properties of the color-singlet processes, which includes their total cross sections, their differential cross sections, and the uncertainties caused by the variation of the e^+e^--collision energy being slightly different from the Z^0-boson mass, by the variation of the heavy quark masses and etc.

	Total cross sections	
production channels	Z^0-propagator	γ^*-propagator
$e^+e^- \to \eta_c(1S) + c\bar{c}$	1.76	4.09×10^{-3}
$e^+e^- \to \eta'_c(2S) + c\bar{c}$	1.11	2.59×10^{-3}
$e^+e^- \to J/\psi(1S) + c\bar{c}$	1.83	4.39×10^{-3}
$e^+e^- \to \psi'(2S) + c\bar{c}$	1.16	2.78×10^{-3}
$e^+e^- \to J/\psi(1S) + gg$	3.84×10^{-2}	6.99×10^{-4}
$e^+e^- \to \psi'(2S) + gg$	2.43×10^{-2}	4.42×10^{-4}
$e^+e^- \to \eta_c(1S) + gg$	1.72×10^{-1}	0
$e^+e^- \to \eta'_c(2S) + gg$	1.09×10^{-1}	0
$e^+e^- \to h_c(1P) + c\bar{c}$	2.34×10^{-1}	5.60×10^{-4}
$e^+e^- \to \chi_{c0}(1P) + c\bar{c}$	3.32×10^{-1}	7.78×10^{-4}
$e^+e^- \to \chi_{c1}(1P) + c\bar{c}$	3.66×10^{-1}	8.37×10^{-4}
$e^+e^- \to \chi_{c2}(1P) + c\bar{c}$	1.44×10^{-1}	3.24×10^{-4}

TABLE II: Total cross section (in unit: pb) for the color-singlet charmnoium production at the Z^0-peak ($\sqrt{S} = m_Z$). The channels are through Z^0 and γ^* propagators respectively. m_c=1.5 GeV.

	Total cross sections	
production channels	Z^0-propagator	γ^*-propagator
$e^+e^- \to \eta_b(1S) + b\bar{b}$	1.94×10^{-1}	8.69×10^{-5}
$e^+e^- \to \eta'_b(2S) + b\bar{b}$	9.60×10^{-2}	4.30×10^{-5}
$e^+e^- \to \Upsilon(1S) + b\bar{b}$	2.18×10^{-1}	1.16×10^{-4}
$e^+e^- \to \Upsilon'(2S) + b\bar{b}$	1.08×10^{-1}	5.74×10^{-5}
$e^+e^- \to \Upsilon(1S) + gg$	6.54×10^{-2}	9.16×10^{-5}
$e^+e^- \to \Upsilon'(2S) + gg$	3.24×10^{-2}	4.53×10^{-5}
$e^+e^- \to \eta_b(1S) + gg$	8.18×10^{-2}	0
$e^+e^- \to \eta'_b(2S) + gg$	4.05×10^{-2}	0
$e^+e^- \to h_b(1P) + b\bar{b}$	6.84×10^{-3}	3.36×10^{-6}
$e^+e^- \to \chi_{b0}(1P) + b\bar{b}$	1.09×10^{-2}	5.18×10^{-6}
$e^+e^- \to \chi_{b1}(1P) + b\bar{b}$	1.04×10^{-2}	4.22×10^{-6}
$e^+e^- \to \chi_{b2}(1P) + b\bar{b}$	4.30×10^{-3}	1.67×10^{-6}

TABLE III: Total cross section (in unit: pb) for the color-singlet bottomonium production at the Z^0-peak ($\sqrt{S} = m_Z$). The channels are through Z^0 or γ^* propagator respectively. m_b=4.9 GeV.

1. *Total and differential cross sections*

Total cross sections for the charmonium and bottomonium productions are presented in Tables II and III. By adding all the P-wave charmonium or bottomonium states together, we obtain

$$\sigma(e^+e^- \to |H_{c\bar{c}}\rangle(1P) + c\bar{c}) \simeq 1.08 \text{ pb}$$

and

$$\sigma(e^+e^- \to |H_{b\bar{b}}\rangle(1P) + b\bar{b}) \simeq 3.25 \times 10^{-2} \text{ pb}.$$

Furthermore, we have $|\Psi_{2S}(0)|^2/|\Psi_{1S}(0)|^2 \sim 0.6$ for charmonium and ~ 0.5 for bottomonium. Then, in addition to the $1S$-level quarkonium states, both the $2S$-level and $1P$-level quarkonium states can provide sizable contributions to the production channel $e^+e^- \to |H_{Q\bar{Q}}\rangle + Q\bar{Q}$.

More explicitly, to show the relative importance of those channels via the Z^0 propagator, we define two type of ratios

$$R_{H_{c\bar{c}}+X} = \frac{\sigma_{e^+e^- \to Z^0 \to |H_{c\bar{c}}\rangle + X}}{\sigma_{e^+e^- \to Z^0 \to J/\psi + c\bar{c}}} \tag{39}$$

and

$$R_{H_{b\bar{b}}+X} = \frac{\sigma_{e^+e^- \to Z^0 \to |H_{b\bar{b}}\rangle + X}}{\sigma_{e^+e^- \to Z^0 \to \Upsilon + b\bar{b}}}. \tag{40}$$

We obtain,

$$R_{\eta_c+gg} = 9.4\% \;,\; R_{\eta'_c+gg} = 6.0\% \;,\; R_{J/\psi+gg} = 2.1\% \;,$$

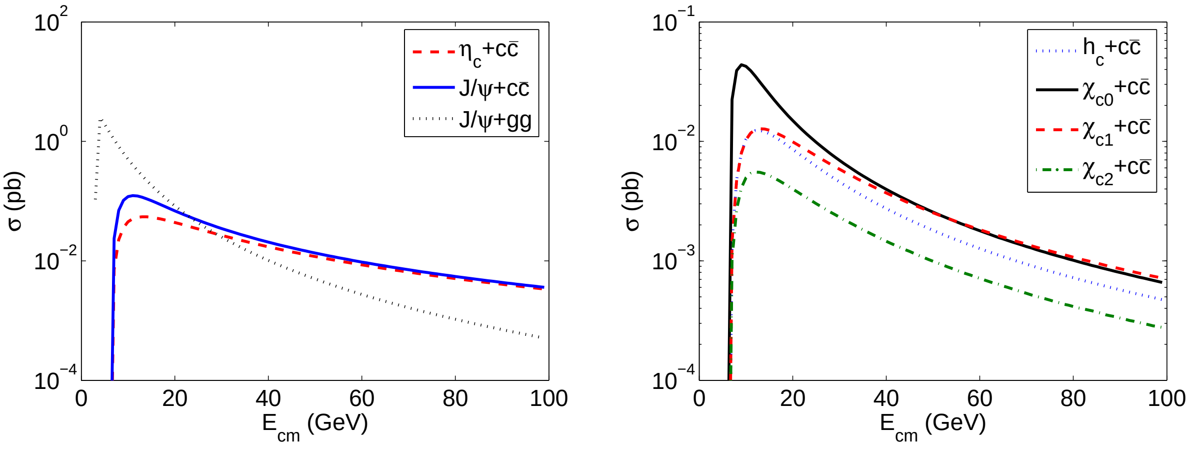

FIG. 6: Total cross sections of the channel $e^+ + e^- \to \gamma^* \to |H_{c\bar{c}}\rangle + X$, including the S wave and P wave charmonium states, versus the e^+e^- collision energy $E_{cm} = \sqrt{S}$.

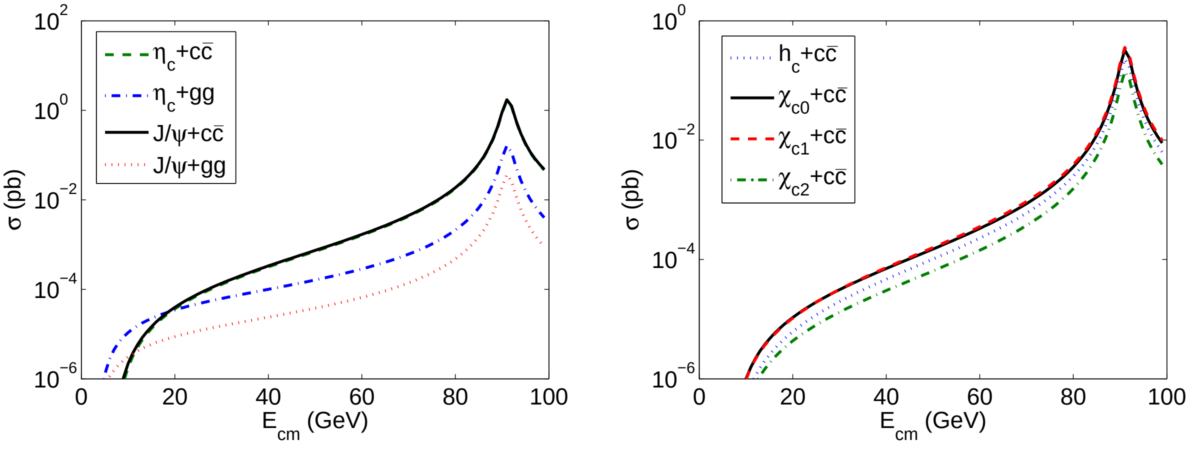

FIG. 7: Total cross sections of the channel $e^+ + e^- \to Z^0 \to |H_{c\bar{c}}\rangle + X$, including the S wave and P wave charmonium states, versus the e^+e^- collision energy $E_{cm} = \sqrt{S}$. The two curves for $\eta_c + c\bar{c}$ and $J/\psi + c\bar{c}$ are almost coincide with each other, and the two curves for $\chi_{c0} + c\bar{c}$ and $\chi_{c1} + c\bar{c}$ are almost coincide with each other.

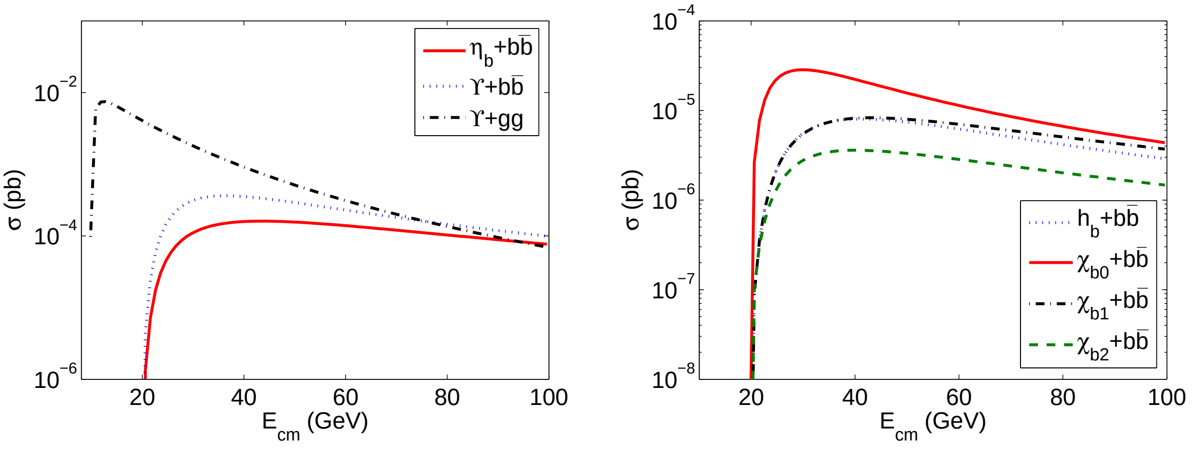

FIG. 8: Total cross sections of the channel $e^+ + e^- \to \gamma^* \to |H_{b\bar{b}}\rangle + X$, including the S wave and P wave bottomonium states, versus the e^+e^- collision energy $E_{cm} = \sqrt{S}$.

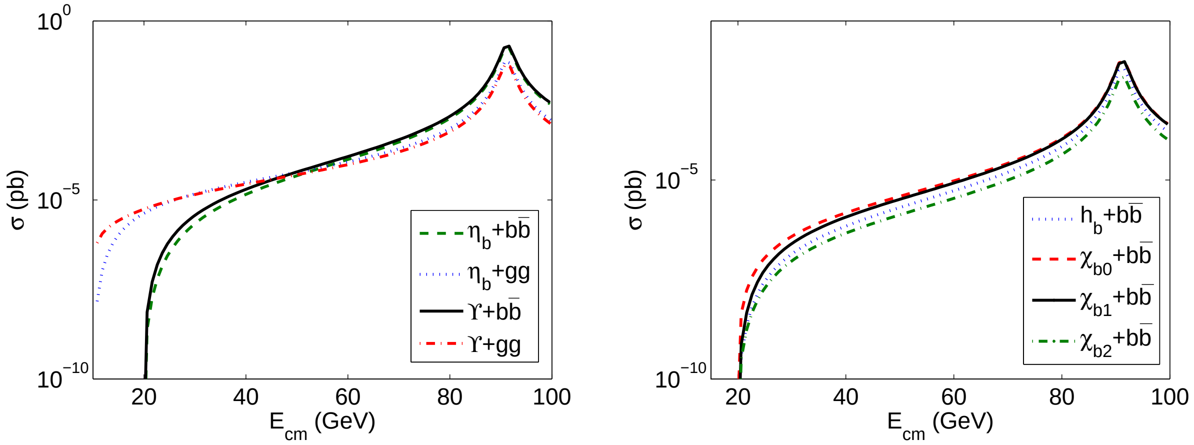

FIG. 9: Total cross sections of the channel $e^+ + e^- \to Z^0 \to |H_{b\bar{b}}\rangle + X$, including the S wave and P wave bottomonium states, versus the e^+e^- collision energy $E_{cm} = \sqrt{S}$. The two curves for $\eta_b + b\bar{b}$ and $\Upsilon + b\bar{b}$ are very close to each other, and the two curves for $\chi_{b0} + b\bar{b}$ and $\chi_{b1} + b\bar{b}$ are very close to each other.

$$\begin{aligned} R_{\psi'+gg} &= 1.3\%\ ,\ R_{\eta_c+c\bar{c}} = 96\%\ ,\ R_{\eta_c'+c\bar{c}} = 61\%\ , \\ R_{\psi'+c\bar{c}} &= 63\%\ ,\ R_{h_c+c\bar{c}} = 13\%\ ,\ R_{\chi_{c0}+c\bar{c}} = 18\%\ , \\ R_{\chi_{c1}+c\bar{c}} &= 20\%\ ,\ R_{\chi_{c2}+c\bar{c}} = 7.8\% \end{aligned}$$

and

$$\begin{aligned} R_{\eta_b+gg} &= 38\%\ ,\ R_{\eta_b'+gg} = 19\%\ ,\ R_{\Upsilon+gg} = 30\%\ , \\ R_{\Upsilon'+gg} &= 15\%\ ,\ R_{\eta_b+b\bar{b}} = 89\%\ ,\ R_{\eta_b'+b\bar{b}} = 44\%\ , \\ R_{\Upsilon'+b\bar{b}} &= 50\%\ ,\ R_{h_b+b\bar{b}} = 3.1\%\ ,\ R_{\chi_{b0}+b\bar{b}} = 5.0\%\ , \\ R_{\chi_{b1}+b\bar{b}} &= 4.8\%\ ,\ R_{\chi_{b2}+b\bar{b}} = 2.0\%. \end{aligned}$$

It has been observed that the Z^0-boson resonance effect will raise the production rate by several orders of magnitude in comparison to the Belle and BABAR experiments, then it could be a better platform for studying the properties of the heavy quarkoniums.

For the e^+e^- collision energy $E_{cm} = \sqrt{S} = m_Z$, the cross sections for the channels via the γ^* propagator are much smaller than those channels via the Z^0 propagator. For example, we have

$$\frac{\sigma_{e^+e^-\to\gamma^*\to J/\psi+c\bar{c}}}{\sigma_{e^+e^-\to Z^0\to J/\psi+c\bar{c}}} = 2.4\times10^{-3}$$

and

$$\frac{\sigma_{e^+e^-\to\gamma^*\to\Upsilon+b\bar{b}}}{\sigma_{e^+e^-\to Z^0\to\Upsilon+b\bar{b}}} = 5.0\times10^{-4}.$$

To show this point clearly, we present the total cross sections for the color-singlet channels versus the collision energy E_{cm} in Figs.(6,7,8,9). In the low collision energy region, the production cross sections are dominated by the cases via the γ^* propagator: main contributions are around $6-20$ GeV for charmonium production and $10-40$ GeV for bottomonium production. While, for the case of Z^0 propagator, it is small in low energy region, but has a peak value at $E_{cm} = m_Z$ due to the Z^0-boson resonance effect. This shows that the Super-Z factory will provide another platform for heavy quarkonium physics in addition to Belle, BarBar, CLEO and LHC colliders.

For the charmonium production channels, from Fig.(7) and Fig.(9), it is found that the total cross sections for $e^+e^- \to Z^0 \to J/\psi + c\bar{c}$ and $e^+e^- \to Z^0 \to \eta_c + c\bar{c}$, and the total cross sections for $e^+e^- \to Z^0 \to \chi_{c0} + c\bar{c}$ and $e^+e^- \to Z^0 \to \chi_{c1} + c\bar{c}$ are almost coincident with each other, especially for larger collision energy. The conditions for the bottomonium cases are similar. This shows there is approximate "spin degeneracy" for the production channels $e^+e^- \to Z^0 \to |H_{Q\bar{Q}}\rangle + Q\bar{Q}$. More clearly, when the collision energy $E_{cm} = m_Z$, we have

$$\frac{\sigma_{e^+e^-\to Z^0\to\eta_c+c\bar{c}}}{\sigma_{e^+e^-\to Z^0\to J/\psi+c\bar{c}}} \simeq 96\% \tag{41}$$

$$\frac{\sigma_{e^+e^-\to Z^0\to\chi_{c0}+c\bar{c}}}{\sigma_{e^+e^-\to Z^0\to\chi_{c1}+c\bar{c}}} \simeq 91\% \tag{42}$$

$$\frac{\sigma_{e^+e^-\to Z^0\to\eta_b+b\bar{b}}}{\sigma_{e^+e^-\to Z^0\to\Upsilon+b\bar{b}}} \simeq 89\% \tag{43}$$

$$\frac{\sigma_{e^+e^-\to Z^0\to\chi_{b1}+b\bar{b}}}{\sigma_{e^+e^-\to Z^0\to\chi_{b0}+b\bar{b}}} \simeq 95\% \tag{44}$$

We present the heavy quarkonium transverse momentum (p_t)-distributions and rapidity (y)-distributions for $E_{cm} = m_Z$ in Figs.(10,11,12,13). These figures show that either for the p_t-distributions or for the y-distributions, the two curves for $e^+e^- \to Z^0 \to J/\psi + c\bar{c}$ and $e^+e^- \to Z^0 \to \eta_c + c\bar{c}$, and the two curves for $e^+e^- \to Z^0 \to \chi_{c0} + c\bar{c}$ and $e^+e^- \to Z^0 \to \chi_{c1} + c\bar{c}$ are also very close to each other. The cures for the bottomonium production are similar.

As a cross check / explanation for the approximate "spin degeneracy", we adopt the fragmentation approach. Using the fragmentation approach the most important/dominant higher-order effects can be included by using the Dokshitzer-Gribov-Lipatov-Altarelli-Parisi

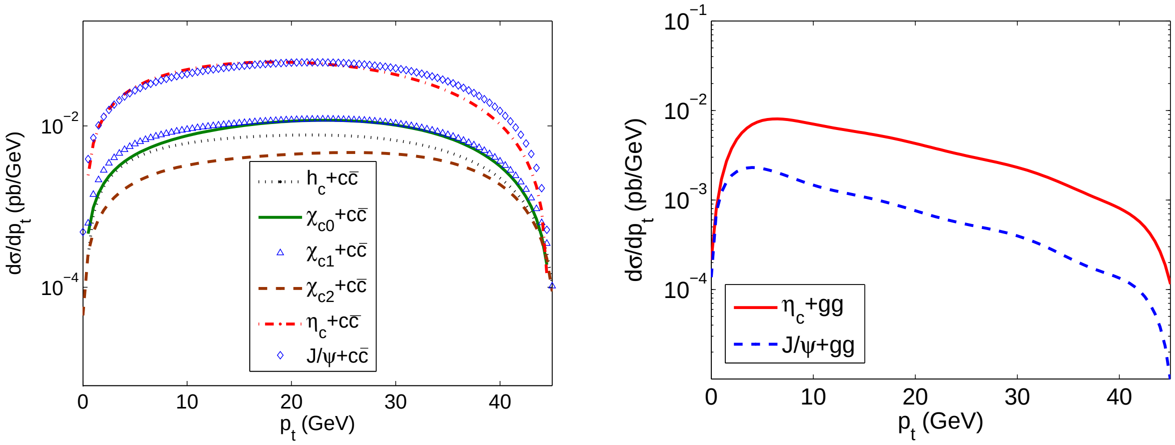

FIG. 10: The charmonium p_t-distributions for the production processes, $e^+e^- \to Z^0 \to |H_{c\bar{c}}\rangle + X$, at the e^+e^- collision energy $E_{cm} = m_Z$. The left is for $X = c\bar{c}$ and the right is for $X = gg$.

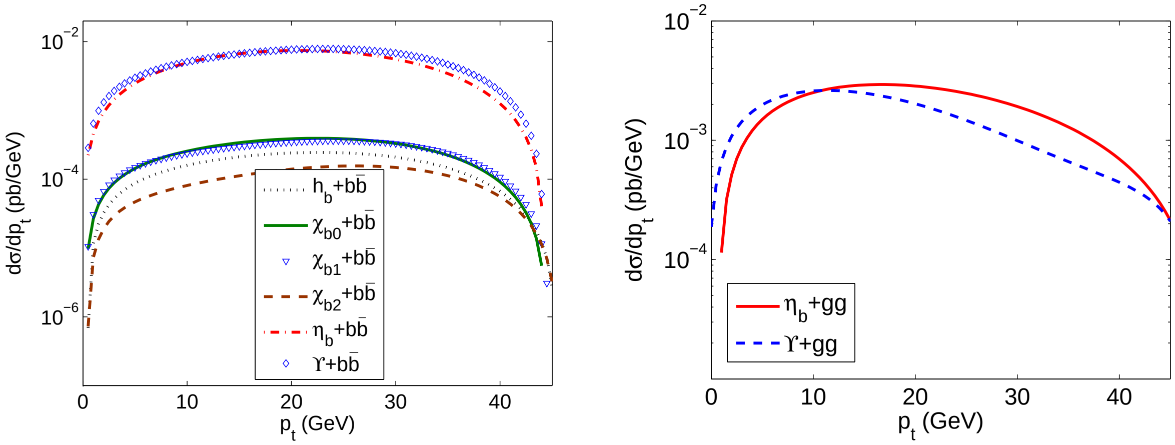

FIG. 11: The bottomonium p_t-distributions for the production processes, $e^+e^- \to Z^0 \to |H_{b\bar{b}}\rangle + X$, at the e^+e^- collision energy $E_{cm} = m_Z$. The left is for $X = b\bar{b}$ and the right is for $X = gg$.

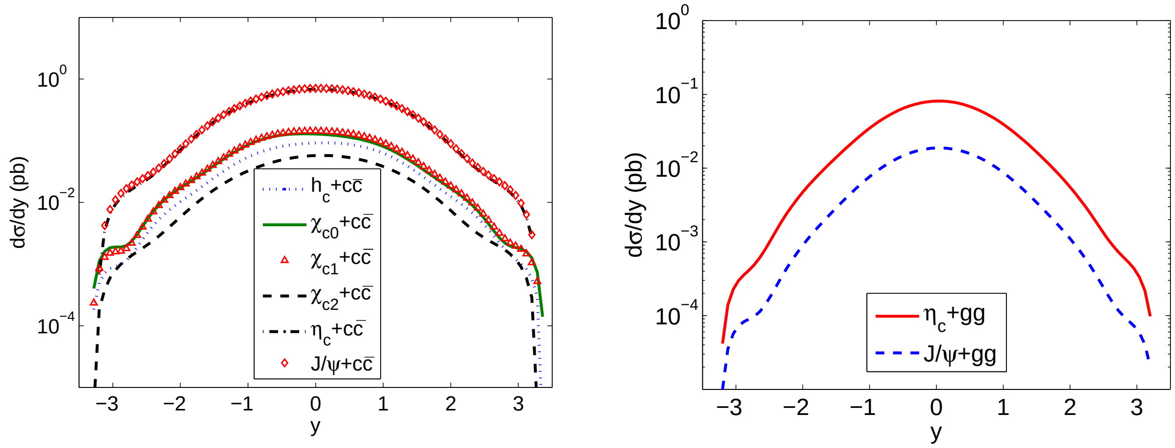

FIG. 12: The charmonium y-distributions for the production processes, $e^+e^- \to Z^0 \to |H_{c\bar{c}}\rangle + X$, at the e^+e^- collision energy $E_{cm} = m_Z$. The left is for $X = c\bar{c}$ and the right is for $X = gg$.

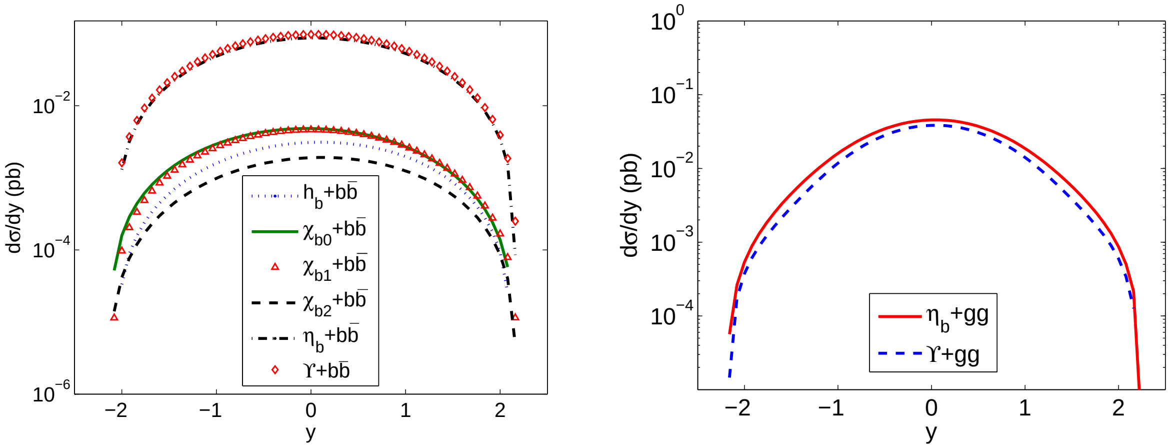

FIG. 13: The bottomonium y-distributions for the production processes, $e^+e^- \to Z^0 \to |H_{b\bar{b}}\rangle + X$, at the e^+e^- collision energy $E_{cm} = m_Z$. The left is for $X = b\bar{b}$ and the right is for $X = gg$.

evolution equation, and the fragmentation approach gives a reasonable approximation to the full tree-level calculation as long as the transverse momentum of the produced heavy hadron is large enough [40–52]. Move over, it has been argued that the fragmentation approach may be extended to lower p_T region under the FONLL scheme [53, 54].

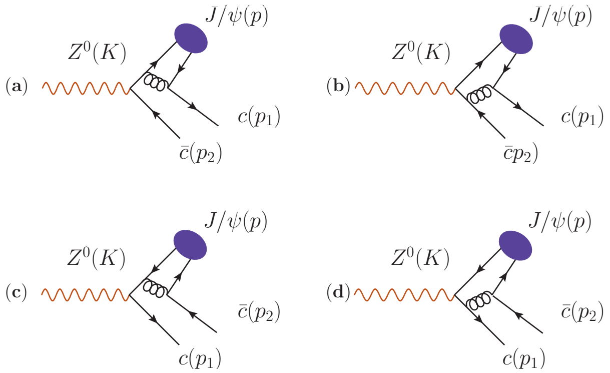

FIG. 14: Feynman diagrams for calculating the total fragmentation probabilities for $c \to J/\psi$ and $c \to \eta_c$.

In the large p_t region, the probability of $Z^0 \to J/\psi$ or η_c is proportional and dominated by the fragmentation of $c \to J/\psi$ or $c \to \eta_c$. For the purpose, we need to deal with the Feynman diagrams shown in Fig.(14). By taking the axial gauge, the amplitudes of Figs.(14b,14d) are suppressed by a factor (m_c/m_Z) in comparison to Figs.(14a,14c), so they are neglected in deriving the fragmentation probabilities for $c \to J/\psi$ and $c \to \eta_c$. Following the same procedure as shown by Ref.[50], one can obtain the total fragmentation probabilities:

$$\int_0^1 \mathrm{d}z D_{c\to J/\psi}(z, 3m_c) = \frac{256}{27}\alpha_s(3m_c)^2 \times \frac{|\Psi_{1S}(0)|^2}{M^3_{J/\psi}} \left(\frac{1189}{30} - 57\ln 2\right), \tag{45}$$

$$\int_0^1 \mathrm{d}z D_{c\to \eta_c}(z, 3m_c) = \frac{256}{27}\alpha_s(3m_c)^2 \times \frac{|\Psi_{1S}(0)|^2}{M^3_{\eta_c}} \left(\frac{773}{30} - 37\ln 2\right), \tag{46}$$

Because

$$\left(\frac{1189}{30} - 57\ln 2\right) \simeq 0.124 \text{ and } \left(\frac{773}{30} - 37\ln 2\right) \simeq 0.120,$$

the ratio of the two fragmentation probabilities is

$$\int_0^1 \mathrm{d}z D_{c\to J/\psi(z,3m_c)} \Big/ \int_0^1 \mathrm{d}z D_{c\to\eta_c}(z, 3m_c) \simeq 97\%.$$

This is consistent with Eq.(41) and clearly shows that there is spin-degeneracy for e^+e^- at the high collision

P_{tcut}(GeV)	5	10	15
$\sigma_{J/\psi(1S)+c\bar{c}}$	1.75(96%)	1.55(85%)	1.29(70%)
$\sigma_{\psi'(2S)+c\bar{c}}$	1.11(96%)	9.81×10^{-1}(85%)	8.17×10^{-1}(70%)
$\sigma_{J/\psi(1S)+gg}$	2.89×10^{-2}(75%)	1.96×10^{-2}(51%)	1.30×10^{-2}(34%)
$\sigma_{\psi'(2S)+gg}$	1.83×10^{-2}(75%)	1.24×10^{-2}(51%)	8.23×10^{-3}(34%)
$\sigma_{\eta_c(1S)+c\bar{c}}$	1.68(95%)	1.46(83%)	1.17(66%)
$\sigma_{\eta'_c(2S)+c\bar{c}}$	1.06(95%)	9.24×10^{-1}(83%)	7.41×10^{-1}(66%)
$\sigma_{\eta_c(1S)+gg}$	1.47×10^{-1}(85%)	1.08×10^{-1}(63%)	7.51×10^{-2}(44%)
$\sigma_{\eta'_c(2S)+gg}$	9.31×10^{-2}(85%)	6.84×10^{-2}(63%)	4.75×10^{-2}(44%)
$\sigma_{h_c(1P)+c\bar{c}}$	2.22×10^{-1}(95%)	1.96×10^{-1}(84%)	1.61×10^{-1}(69%)
$\sigma_{\chi_{c0}(1P)+c\bar{c}}$	3.17×10^{-1}(95%)	2.86×10^{-1}(86%)	2.42×10^{-1}(73%)
$\sigma_{\chi_{c1}(1P)+c\bar{c}}$	3.46×10^{-1}(94%)	3.08×10^{-1}(84%)	2.56×10^{-1}(70%)
$\sigma_{\chi_{c2}(1P)+c\bar{c}}$	1.37×10^{-1}(95%)	1.24×10^{-1}(86%)	1.05×10^{-1}(73%)

TABLE IV: Cross section (in unit: pb) for the color-singlet charmonium production at the Z^0-peak ($\sqrt{S}=m_Z$) with different P_{tcut}. The channels are through Z^0 propagator. m_c=1.5 GeV. Here the percentages in the parentheses represent the ratios between the cross sections with various P_{tcut} and the one without P_t cut.

P_{tcut}(GeV)	5	10	15
$\sigma_{\Upsilon(1S)+b\bar{b}}$	2.10×10^{-1}(96%)	1.89×10^{-1}(87%)	1.59×10^{-1}(73%)
$\sigma_{\Upsilon'(2S)+b\bar{b}}$	1.04×10^{-1}(96%)	9.35×10^{-2}(87%)	7.86×10^{-2}(73%)
$\sigma_{\Upsilon(1S)+gg}$	5.90×10^{-2}(90%)	4.63×10^{-2}(71%)	3.37×10^{-2}(51%)
$\sigma_{\Upsilon'(2S)+gg}$	2.92×10^{-2}(90%)	2.29×10^{-2}(71%)	1.67×10^{-2}(51%)
$\sigma_{\eta_b(1S)+b\bar{b}}$	1.88×10^{-1}(97%)	1.68×10^{-1}(87%)	1.38×10^{-1}(71%)
$\sigma_{\eta'_b(2S)+b\bar{b}}$	9.30×10^{-2}(97%)	8.31×10^{-2}(87%)	6.83×10^{-2}(71%)
$\sigma_{\eta_b(1S)+gg}$	7.85×10^{-2}(96%)	6.80×10^{-2}(83%)	5.35×10^{-2}(65%)
$\sigma_{\eta'_b(2S)+gg}$	3.88×10^{-2}(96%)	3.36×10^{-2}(83%)	2.65×10^{-2}(65%)
$\sigma_{h_b(1P)+b\bar{b}}$	6.60×10^{-3}(96%)	6.00×10^{-3}(88%)	5.00×10^{-3}(73%)
$\sigma_{\chi_{b0}(1P)+b\bar{b}}$	1.05×10^{-2}(96%)	9.40×10^{-3}(86%)	7.85×10^{-3}(72%)
$\sigma_{\chi_{b1}(1P)+b\bar{b}}$	9.95×10^{-3}(96%)	8.95×10^{-3}(86%)	7.60×10^{-3}(73%)
$\sigma_{\chi_{b2}(1P)+b\bar{b}}$	4.16×10^{-3}(97%)	3.84×10^{-3}(89%)	3.33×10^{-3}(77%)

TABLE V: Cross section (in unit: pb) for the color-singlet bottomonium production at the Z^0-peak ($\sqrt{S}=m_Z$) with different P_{tcut}. The channels are through Z^0 propagator. m_b=4.9 GeV. Here the percentages in the parentheses represent the ratios between the cross sections with various P_{tcut} and the one without P_t cut.

energy. Using these expressions, one can conveniently obtain the total fragmentation probabilities for $b\to\Upsilon$ and $b\to\eta_b$ by changing m_c into m_b. More over, the P-wave case can be derived through a similar way, whose detailed derivations can be found in Ref.[52], and we can obtain similar conclusions.

In experiment, no detector can cover all the kinematics of the events, so only some of the H_c or H_b events can be observed. That is, the events with small p_t and /or a large rapidity y cannot be detected. So, the cross sections

y_{cut}	0.5	1.0	1.5
$\sigma_{J/\psi(1S)+c\bar{c}}$	7.00×10^{-1}(38%)	1.27(69%)	1.60(87%)
$\sigma_{\psi'(2S)+c\bar{c}}$	4.43×10^{-1}(38%)	8.04×10^{-1}(69%)	1.01(87%)
$\sigma_{J/\psi(1S)+gg}$	1.82×10^{-2}(47%)	3.02×10^{-2}(79%)	3.58×10^{-2}(93%)
$\sigma_{\psi'(2S)+gg}$	1.15×10^{-2}(47%)	1.91×10^{-2}(79%)	2.27×10^{-2}(93%)
$\sigma_{\eta_c(1S)+c\bar{c}}$	6.71×10^{-1}(38%)	1.23(70%)	1.55(88%)
$\sigma_{\eta'_c(2S)+c\bar{c}}$	4.25×10^{-1}(38%)	7.79×10^{-1}(70%)	9.81×10^{-1}(88%)
$\sigma_{\eta_c(1S)+gg}$	7.88×10^{-2}(46%)	1.32×10^{-1}(77%)	1.58×10^{-1}(92%)
$\sigma_{\eta'_c(2S)+gg}$	4.99×10^{-2}(46%)	8.36×10^{-2}(77%)	1.00×10^{-1}(92%)
$\sigma_{h_c(1P)+c\bar{c}}$	8.97×10^{-2}(38%)	1.63×10^{-1}(70%)	2.05×10^{-1}(88%)
$\sigma_{\chi_{c0}(1P)+c\bar{c}}$	1.25×10^{-1}(38%)	2.28×10^{-1}(68%)	2.88×10^{-1}(86%)
$\sigma_{\chi_{c1}(1P)+c\bar{c}}$	1.39×10^{-1}(38%)	2.53×10^{-1}(69%)	3.20×10^{-1}(87%)
$\sigma_{\chi_{c2}(1P)+c\bar{c}}$	5.48×10^{-2}(38%)	9.97×10^{-2}(69%)	1.25×10^{-1}(87%)

TABLE VI: Cross section (in unit: pb) for the color-singlet charmonium production at the Z^0-peak ($\sqrt{S}=m_Z$) with different y_{cut}. The channels are through Z^0 propagator. m_c=1.5 GeV. Here the percentages in the parentheses represent the ratios between the cross sections with various y_{cut} and the one without rapidity cut.

y_{cut}	0.5	1.0	1.5
$\sigma_{\Upsilon(1S)+b\bar{b}}$	9.40×10^{-2}(43%)	1.67×10^{-1}(77%)	2.06×10^{-1}(94%)
$\sigma_{\Upsilon'(2S)+b\bar{b}}$	4.65×10^{-2}(43%)	8.26×10^{-2}(77%)	1.02×10^{-1}(94%)
$\sigma_{\Upsilon(1S)+gg}$	3.54×10^{-2}(54%)	5.63×10^{-2}(86%)	6.38×10^{-2}(98%)
$\sigma_{\Upsilon'(2S)+gg}$	1.75×10^{-2}(54%)	2.78×10^{-2}(86%)	3.16×10^{-2}(98%)
$\sigma_{\eta_b(1S)+b\bar{b}}$	8.26×10^{-2}(43%)	1.49×10^{-1}(77%)	1.84×10^{-1}(95%)
$\sigma_{\eta'_b(2S)+b\bar{b}}$	4.09×10^{-2}(43%)	7.37×10^{-2}(77%)	9.10×10^{-2}(95%)
$\sigma_{\eta_b(1S)+gg}$	4.23×10^{-2}(52%)	6.87×10^{-2}(84%)	7.92×10^{-2}(97%)
$\sigma_{\eta'_b(2S)+gg}$	2.09×10^{-2}(52%)	3.40×10^{-2}(84%)	3.92×10^{-2}(97%)
$\sigma_{h_b(1P)+b\bar{b}}$	3.01×10^{-3}(44%)	5.29×10^{-3}(77%)	6.48×10^{-3}(95%)
$\sigma_{\chi_{b0}(1P)+b\bar{b}}$	4.60×10^{-3}(42%)	8.26×10^{-3}(76%)	1.02×10^{-2}(94%)
$\sigma_{\chi_{b1}(1P)+b\bar{b}}$	4.47×10^{-3}(43%)	7.93×10^{-3}(76%)	9.77×10^{-3}(94%)
$\sigma_{\chi_{b2}(1P)+b\bar{b}}$	1.84×10^{-3}(43%)	3.27×10^{-3}(76%)	4.02×10^{-3}(93%)

TABLE VII: Cross section (in unit: pb) for the color-singlet bottomonium production at the Z^0-peak ($\sqrt{S}=m_Z$) with different y_{cut}. The channels are through Z^0 propagator. m_b=4.9 GeV. Here the percentages in the parentheses represent the ratios between the cross sections with various y_{cut} and the one without rapidity cut.

with different p_{tcut} and y_{cut} are presented in Table IV, TableV, TableVI and TableVII.

2. Uncertainties caused by the variation of E_{cm} and m_Q

For the leading-order calculation, the uncertainty sources include the bound-state matrix elements, the renormalization scale, the quark masses m_b and m_c, and etc.. The conventional scale-setting assigns the typical momentum flow of the process as the renormalization scale, e.g. $2m_c$ for charmonium production and $2m_b$ for bottomonium production. This *ad hoc* assignment of scale and its range leads to an important systematic error in the present theoretical estimations. In the literature, the principle of maximum conformality (PMC) [55] provides a feasible way to derive a precise QCD predictions. The main idea of PMC is to sum all the non-conformal β-terms in the perturbative expansion into the running coupling, and then the remaining terms are identical to that of a conformal theory. The PMC estimation is then scheme independent, and the remaining scale dependence can be greatly suppressed. At the present, the matrix elements and the strong coupling constant α_s emerge as overall factors and their uncertainties can be conveniently discussed when we know their values well, so we will not discuss their uncertainties in the present paper.

As shown in the last subsection, if the collision energy E_{cm} is around m_Z, the total cross sections for the channels via the γ^* propagator are much smaller than those of the channels via the Z^0 propagator. In the present subsection, we will adopt the channel via the Z^0-propagator

E_{cm}	97% m_Z	m_Z	103% m_Z
$\sigma_{J/\psi+gg}$	6.66×10^{-3}	3.84×10^{-2}	6.57×10^{-3}
$\sigma_{\psi'+gg}$	4.22×10^{-3}	2.43×10^{-2}	4.16×10^{-3}
σ_{η_c+gg}	2.97×10^{-2}	1.72×10^{-1}	2.94×10^{-2}
$\sigma_{\eta_c'+gg}$	1.88×10^{-2}	1.09×10^{-1}	1.86×10^{-2}
$\sigma_{J/\psi+c\bar{c}}$	3.02×10^{-1}	1.83	3.26×10^{-1}
$\sigma_{\psi'+c\bar{c}}$	1.91×10^{-1}	1.16	2.06×10^{-1}
$\sigma_{\eta_c+c\bar{c}}$	2.91×10^{-1}	1.76	3.14×10^{-1}
$\sigma_{\eta_c'+c\bar{c}}$	1.84×10^{-1}	1.11	1.99×10^{-1}
$\sigma_{h_c+c\bar{c}}$	3.88×10^{-2}	2.34×10^{-1}	4.18×10^{-2}
$\sigma_{\chi_{c0}+c\bar{c}}$	5.51×10^{-2}	3.32×10^{-1}	5.92×10^{-2}
$\sigma_{\chi_{c1}+c\bar{c}}$	6.08×10^{-2}	3.66×10^{-1}	6.55×10^{-2}
$\sigma_{\chi_{c2}+c\bar{c}}$	2.40×10^{-2}	1.44×10^{-1}	2.59×10^{-2}

TABLE VIII: Total cross sections (in unit: pb) for the production channel $e^+e^-\to Z^0\to|H_{c\bar{c}}\rangle+X$.

E_{cm}	97% m_Z	m_Z	103% m_Z
$\sigma_{\Upsilon+gg}$	1.12×10^{-2}	6.54×10^{-2}	1.13×10^{-2}
$\sigma_{\Upsilon'+gg}$	5.54×10^{-3}	3.24×10^{-2}	5.59×10^{-3}
σ_{η_b+gg}	1.40×10^{-2}	8.18×10^{-2}	1.42×10^{-2}
$\sigma_{\eta_b'+gg}$	6.93×10^{-3}	4.05×10^{-2}	7.03×10^{-3}
$\sigma_{\Upsilon+b\bar{b}}$	3.57×10^{-2}	2.18×10^{-1}	3.95×10^{-2}
$\sigma_{\Upsilon'+b\bar{b}}$	1.77×10^{-2}	1.08×10^{-1}	1.95×10^{-2}
$\sigma_{\eta_b+b\bar{b}}$	3.17×10^{-2}	1.94×10^{-1}	3.53×10^{-2}
$\sigma_{\eta_b'+b\bar{b}}$	1.57×10^{-2}	9.60×10^{-2}	1.75×10^{-2}
$\sigma_{h_b+b\bar{b}}$	1.13×10^{-3}	6.84×10^{-3}	1.24×10^{-3}
$\sigma_{\chi_{b0}+b\bar{b}}$	1.80×10^{-3}	1.09×10^{-2}	1.95×10^{-3}
$\sigma_{\chi_{b1}+b\bar{b}}$	1.71×10^{-3}	1.04×10^{-2}	1.88×10^{-3}
$\sigma_{\chi_{b2}+b\bar{b}}$	7.06×10^{-4}	4.30×10^{-3}	7.74×10^{-4}

TABLE IX: Total cross sections (in unit: pb) for the production channel $e^+e^-\to Z^0\to|H_{b\bar{b}}\rangle+X$.

m_c GeV	1.35 GeV	1.65 GeV	uncertainty
$\sigma_{J/\psi+gg}$	4.55×10^{-2}	3.29×10^{-2}	$^{+0.007}_{-0.006}$
$\sigma_{\psi'+gg}$	2.88×10^{-2}	2.08×10^{-2}	$^{+0.005}_{-0.004}$
σ_{η_c+gg}	2.04×10^{-1}	1.46×10^{-1}	$^{+0.032}_{-0.026}$
$\sigma_{\eta_c'+gg}$	1.29×10^{-1}	9.24×10^{-2}	$^{+0.020}_{-0.017}$
$\sigma_{J/\psi+c\bar{c}}$	2.53	1.36	$^{+0.700}_{-0.470}$
$\sigma_{\psi'+c\bar{c}}$	1.60	8.61×10^{-1}	$^{+0.440}_{-0.299}$
$\sigma_{\eta_c+c\bar{c}}$	2.44	1.31	$^{+0.680}_{-0.450}$
$\sigma_{\eta_c'+c\bar{c}}$	1.54	8.29×10^{-1}	$^{+0.430}_{-0.281}$
$\sigma_{h_c+c\bar{c}}$	3.99×10^{-1}	1.45×10^{-1}	$^{+0.165}_{-0.089}$
$\sigma_{\chi_{c0}+c\bar{c}}$	5.64×10^{-1}	2.04×10^{-1}	$^{+0.232}_{-0.128}$
$\sigma_{\chi_{c1}+c\bar{c}}$	6.25×10^{-1}	2.26×10^{-1}	$^{+0.259}_{-0.140}$
$\sigma_{\chi_{c2}+c\bar{c}}$	2.44×10^{-1}	8.90×10^{-2}	$^{+0.100}_{-0.055}$

TABLE X: Total cross sections (in unit: pb) for the channel $e^+e^-\to Z^0\to|H_{c\bar{c}}\rangle+X$ by setting $m_c=1.50\pm0.15$ GeV. The final column presents the uncertainties from the center values under $m_c=1.5$ GeV.

m_b(GeV)	4.75GeV	5.05GeV	uncertainty
$\sigma_{\Upsilon+gg}$	6.95×10^{-2}	6.17×10^{-2}	$^{+0.004}_{-0.003}$
$\sigma_{\Upsilon'+gg}$	3.44×10^{-2}	3.05×10^{-2}	$^{+0.002}_{-0.002}$
σ_{η_b+gg}	8.72×10^{-2}	7.69×10^{-2}	$^{+0.005}_{-0.005}$
$\sigma_{\eta_b'+gg}$	4.32×10^{-2}	3.81×10^{-2}	$^{+0.003}_{-0.002}$
$\sigma_{\Upsilon+b\bar{b}}$	2.43×10^{-1}	1.96×10^{-1}	$^{+0.025}_{-0.022}$
$\sigma_{\Upsilon'+b\bar{b}}$	1.20×10^{-1}	9.70×10^{-2}	$^{+0.012}_{-0.011}$
$\sigma_{\eta_b+b\bar{b}}$	2.17×10^{-1}	1.74×10^{-1}	$^{+0.023}_{-0.020}$
$\sigma_{\eta_b'+b\bar{b}}$	1.07×10^{-1}	8.61×10^{-2}	$^{+0.011}_{-0.010}$
$\sigma_{h_b+b\bar{b}}$	8.12×10^{-3}	5.83×10^{-3}	$^{+0.001}_{-0.001}$
$\sigma_{\chi_{b0}+b\bar{b}}$	1.28×10^{-2}	9.31×10^{-3}	$^{+0.002}_{-0.002}$
$\sigma_{\chi_{b1}+b\bar{b}}$	1.23×10^{-2}	8.87×10^{-3}	$^{+0.002}_{-0.002}$
$\sigma_{\chi_{b2}+b\bar{b}}$	5.09×10^{-3}	3.67×10^{-3}	$^{+0.001}_{-0.001}$

TABLE XI: Total cross sections (in unit: pb) for the channel $e^+e^-\to Z^0\to|H_{b\bar{b}}\rangle+X$ by setting $m_b=4.90\pm0.15$ GeV. The final column presents the uncertainties from the center values under $m_b=4.90$ GeV.

to do our following discussion, i.e. to deal with the channel $e^+e^-\to Z^0\to|H_{Q\bar{Q}}\rangle+X$. For clarity, to discuss the uncertainty from any one parameter, we will take others to be their center values.

To show the sensitivity of the total cross sections to the collision energy around the Z^0 peak, we calculate the total cross sections by taking $E_{cm}=(1\pm3\%)m_Z$. Our results are presented in Tables VIII and IX.

By varying E_{cm} within the range of $(1\pm3\%)m_Z$, the total cross sections change greatly: e.g. it is down to $\binom{18\%}{17\%}$ of its peak value for $e^+e^-\to Z^0\to J/\psi+c\bar{c}$; while for the channel $e^+e^-\to Z^0\to\Upsilon+b\bar{b}$, it is down to $\binom{18\%}{16\%}$.

Next, we discuss the uncertainties from the heavy quark masses by varying $m_c=1.50\pm0.15$ GeV and $m_b=4.9\pm0.15$ GeV respectively. Our results for $e^+e^-\to Z^0\to|H_{Q\bar{Q}}\rangle+X$ are presented in Tables X and XI. These tables show

- For the charmonium production, when $X=c\bar{c}$, the uncertainties caused by varying $m_c=1.50\pm0.15$ GeV are $\sim40\%$ for the S-wave case, which change to be $\sim70\%$ for the P-wave case; when $X=gg$, the uncertainties for both the S-wave and P-wave cases are $\sim15\%-19\%$.
- For the bottominum production, when $X=b\bar{b}$, the uncertainties caused by varying $m_b=4.90\pm0.15$ GeV are $\sim11\%$ for the S-wave case, which change to be $\sim15\%-18\%$ for the P-wave case; when $X=gg$, the uncertainties for both the S-wave and P-wave cases are $\sim6\%$.

B. Properties of the color-octet processes

1. Total cross sections

As discussed in the introduction, we will discuss the following sizeable color-octet processes

$$\begin{aligned}
e^+e^- \to Z^0 &\to |(Q\bar{Q})[\Big(1^1S_0^{(\mathbf{8})}\Big),\Big(1^3S_1^{(\mathbf{8})}\Big)]g\rangle + Q\bar{Q} \\
&\to \psi_Q + Q\bar{Q}\ , \\
e^+e^- \to Z^0 &\to |(Q\bar{Q})[\Big(1^1S_0^{(\mathbf{8})}\Big)]g\rangle + Q\bar{Q} \to h_Q + Q\bar{Q}\ , \\
e^+e^- \to Z^0 &\to |(Q\bar{Q})[\Big(1^3S_1^{(\mathbf{8})}\Big)]g\rangle + Q\bar{Q} \to \chi_{QJ} + Q\bar{Q}
\end{aligned}$$

and

$$\begin{aligned}
e^+e^- \to Z^0 &\to |(Q\bar{Q})[\Big(1^1S_0^{(\mathbf{8})}\Big),\Big(1^3S_1^{(\mathbf{8})}\Big)]g\rangle + g\ , \\
&\to \psi_Q + g \\
e^+e^- \to Z^0 &\to |(Q\bar{Q})[\Big(1^1S_0^{(\mathbf{8})}\Big)]g\rangle + g \to h_Q + g\ , \\
e^+e^- \to Z^0 &\to |(Q\bar{Q})[\Big(1^3S_1^{(\mathbf{8})}\Big)]g\rangle + g \to \chi_{QJ} + g.
\end{aligned}$$

It is noted that the total cross sections for the color-octet channels versus the collision energy have similar shapes with Figs.(6,7,8,9).

We present their total cross sections at the e^+e^- collision energy E_{cm} in Tables XII and XIII. For the channels of $X = c\bar{c}$ or $b\bar{b}$, Table XII shows

$$\begin{aligned}
\frac{\sigma(e^+e^- \to Z^0 \to |(c\bar{c})[(1^1S_0^{(\mathbf{8})})]g\rangle + X \to J/\psi + X)}{\sigma(e^+e^- \to Z^0 \to |(c\bar{c})[(1^3S_1^{(\mathbf{1})})]\rangle + X \to J/\psi + X)} &= 0.1\%, \\
\frac{\sigma(e^+e^- \to Z^0 \to |(c\bar{c})[(1^3S_1^{(\mathbf{8})})]g\rangle + X \to J/\psi + X)}{\sigma(e^+e^- \to Z^0 \to |(c\bar{c})[(1^3S_1^{(\mathbf{1})})]\rangle + X \to J/\psi + X)} &= 50\%, \\
\frac{\sigma(e^+e^- \to Z^0 \to |(b\bar{b})[(1^1S_0^{(\mathbf{8})})]g\rangle + X \to \Upsilon + X)}{\sigma(e^+e^- \to Z^0 \to |(b\bar{b})[(1^3S_1^{(\mathbf{1})})]\rangle + X \to \Upsilon + X)} &= 0.01\%, \\
\frac{\sigma(e^+e^- \to Z^0 \to |(b\bar{b})[(1^3S_1^{(\mathbf{8})})]g\rangle + X \to \Upsilon + X)}{\sigma(e^+e^- \to Z^0 \to |(b\bar{b})[(1^3S_1^{(\mathbf{1})})]\rangle + X \to \Upsilon + X)} &= 1.9\%
\end{aligned}$$

and Table XIII shows

$$\begin{aligned}
\frac{\sigma(e^+e^- \to Z^0 \to |(c\bar{c})[(1^1S_0^{(\mathbf{8})})]g\rangle + X \to h_c + X)}{\sigma(e^+e^- \to Z^0 \to |(c\bar{c})[(1^1P_1^{(\mathbf{1})})]\rangle + X \to h_c + X)} &= 2.9\%, \\
\frac{\sigma(e^+e^- \to Z^0 \to |(c\bar{c})[(1^3S_1^{(\mathbf{8})})]g\rangle + X \to \chi_{cJ} + X)}{\sigma(e^+e^- \to Z^0 \to |(c\bar{c})[(1^3P_J^{(\mathbf{1})})]\rangle + X \to \chi_{cJ} + X)} &= 433\%, \\
\frac{\sigma(e^+e^- \to Z^0 \to |(b\bar{b})[(1^1S_0^{(\mathbf{8})})]g\rangle + X \to h_b + X)}{\sigma(e^+e^- \to Z^0 \to |(b\bar{b})[(1^1P_1^{(\mathbf{1})})]\rangle + X \to h_b + X)} &= 5.5\%, \\
\frac{\sigma(e^+e^- \to Z^0 \to |(b\bar{b})[(1^3S_1^{(\mathbf{8})})]g\rangle + X \to \chi_{bJ} + X)}{\sigma(e^+e^- \to Z^0 \to |(b\bar{b})[(1^3P_J^{(\mathbf{1})})]\rangle + X \to \chi_{bJ} + X)} &= 173\%.
\end{aligned}$$

And the ratios for the case of $X = g$ are similar.

We make a discussion of the relative importance of different channels at the super Z factory with $E_{cm} = m_Z$ and at the B factory with $E_{cm} = 10.6$ GeV :

- At the super Z factory, the channel $e^+e^- \to Z^0 \to |(Q\bar{Q})[\Big(1^3S_1^{(\mathbf{8})}\Big)]g\rangle + Q\bar{Q}$ provides dominant contribution over other octet channels, due to the topology of Fig.(4c). While, at the B factory, the quarkonium production is dominant by the channel via the γ^* propagator, we will not have such big enhancement; i.e., we have

J/ψ or Υ production channels	$\sigma_{(a)}$	$\sigma_{(b)}$	$\sigma_{(c)}$	$\sigma_{\rm tot}$
$e^+e^- \to Z^0 \to \vert(c\bar{c})[(1^1S_0^{(\mathbf{8})})]g\rangle + c\bar{c} \to J/\psi + c\bar{c}$	1.65×10^{-3}	2.65×10^{-5}	$\sim$	1.69×10^{-3}
$e^+e^- \to Z^0 \to \vert(c\bar{c})[(1^3S_1^{(\mathbf{8})})]g\rangle + c\bar{c} \to J/\psi + c\bar{c}$	1.71×10^{-3}	1.80×10^{-4}	8.92×10^{-1}	9.11×10^{-1}
$e^+e^- \to Z^0 \to \vert(c\bar{c})[(1^1S_0^{(\mathbf{8})})]g\rangle + g \to J/\psi + g$	$\sim$	$\sim$	$\sim$	4.87×10^{-4}
$e^+e^- \to Z^0 \to \vert(c\bar{c})[(1^3S_1^{(\mathbf{8})})]g\rangle + g \to J/\psi + g$	$\sim$	$\sim$	$\sim$	3.31×10^{-3}
$e^+e^- \to Z^0 \to \vert(b\bar{b})[(1^1S_0^{(\mathbf{8})})]g\rangle + b\bar{b} \to \Upsilon + b\bar{b}$	1.86×10^{-5}	5.22×10^{-6}	$\sim$	2.76×10^{-5}
$e^+e^- \to Z^0 \to \vert(b\bar{b})[(1^3S_1^{(\mathbf{8})})]g\rangle + b\bar{b} \to \Upsilon + b\bar{b}$	2.09×10^{-5}	1.13×10^{-5}	4.05×10^{-3}	4.23×10^{-3}
$e^+e^- \to Z^0 \to \vert(b\bar{b})[(1^1S_0^{(\mathbf{8})})]g\rangle + g \to \Upsilon + g$	$\sim$	$\sim$	$\sim$	2.81×10^{-4}
$e^+e^- \to Z^0 \to \vert(b\bar{b})[(1^3S_1^{(\mathbf{8})})]g\rangle + g \to \Upsilon + g$	$\sim$	$\sim$	$\sim$	5.93×10^{-4}

TABLE XII: Total cross sections (in unit: pb) for the color-octet heavy quarkonium production via the e^+e^- annihilation at $E_{cm}=Z^0$, where the subscripts (a), (b) and (c) stand for Feynman figures shown in Figs.(3,4) respectively. The symbol $\sigma_{\rm tot}$ refers to the sum of $\sigma_{(a)}$, $\sigma_{(b)}$, $\sigma_{(c)}$ and their interference terms for the channel $e^+e^- \to Z^0 \to |(Q\bar{Q})[\left(1^1S_0^{(\mathbf{8})}\right), \left(1^3S_1^{(\mathbf{8})}\right)]g\rangle + Q\bar{Q}$; and it refers to the cross section of Fig.(5) for the channel $e^+e^- \to Z^0 \to |(Q\bar{Q})[\left(1^1S_0^{(\mathbf{8})}\right), \left(1^3S_1^{(\mathbf{8})}\right)]g\rangle + g$.

$h_c(h_b)$ or $\chi_{cJ}(\chi_{bJ})$ production channels	$\sigma_{(a)}$	$\sigma_{(b)}$	$\sigma_{(c)}$	$\sigma_{\rm tot}$
$e^+e^- \to Z^0 \to \vert(c\bar{c})[(1^1S_0^{(\mathbf{8})})]g\rangle + c\bar{c} \to h_c + c\bar{c}$	6.59×10^{-3}	1.06×10^{-4}	$\sim$	6.78×10^{-3}
$e^+e^- \to Z^0 \to \vert(c\bar{c})[(1^3S_1^{(\mathbf{8})})]g\rangle + c\bar{c} \to \chi_{cJ} + c\bar{c}$	6.85×10^{-3}	7.21×10^{-4}	3.56	3.65
$e^+e^- \to Z^0 \to \vert(c\bar{c})[(1^1S_0^{(\mathbf{8})})]g\rangle + g \to h_c + g$	$\sim$	$\sim$	$\sim$	1.95×10^{-3}
$e^+e^- \to Z^0 \to \vert(c\bar{c})[(1^3S_1^{(\mathbf{8})})]g\rangle + g \to \chi_{cJ} + g$	$\sim$	$\sim$	$\sim$	1.32×10^{-2}
$e^+e^- \to Z^0 \to \vert(b\bar{b})[(1^1S_0^{(\mathbf{8})})]g\rangle + b\bar{b} \to h_b + b\bar{b}$	2.53×10^{-4}	7.09×10^{-5}	$\sim$	3.75×10^{-4}
$e^+e^- \to Z^0 \to \vert(b\bar{b})[(1^3S_1^{(\mathbf{8})})]g\rangle + b\bar{b} \to \chi_{bJ} + b\bar{b}$	2.09×10^{-4}	1.53×10^{-4}	4.26×10^{-2}	4.44×10^{-2}
$e^+e^- \to Z^0 \to \vert(b\bar{b})[(1^1S_0^{(\mathbf{8})})]g\rangle + g \to h_b + g$	$\sim$	$\sim$	$\sim$	3.81×10^{-3}
$e^+e^- \to Z^0 \to \vert(b\bar{b})[(1^3S_1^{(\mathbf{8})})]g\rangle + g \to \chi_{bJ} + g$	$\sim$	$\sim$	$\sim$	8.05×10^{-3}

TABLE XIII: Total cross sections (in unit: pb) for the color-octet heavy quarkonium production via the e^+e^- annihilation at $E_{cm}=Z^0$, where the subscripts (a), (b) and (c) stand for Feynman figures shown in Figs.(3,4) respectively. The symbol $\sigma_{\rm tot}$ refers to the sum of $\sigma_{(a)}$, $\sigma_{(b)}$, $\sigma_{(c)}$ and their interference terms for the channel $e^+e^- \to Z^0 \to |(Q\bar{Q})[\left(1^1S_0^{(\mathbf{8})}\right), \left(1^3S_1^{(\mathbf{8})}\right)]g\rangle + Q\bar{Q}$; and it refers to the cross section of Fig.(5) for the channel $e^+e^- \to Z^0 \to |(Q\bar{Q})[\left(1^1S_0^{(\mathbf{8})}\right), \left(1^3S_1^{(\mathbf{8})}\right)]g\rangle + g$. Here the contributions to ${}^3P_0, {}^3P_1, {}^3P_2$ from color octet component $(Q\bar{Q})[(1^3S_1^{(\mathbf{8})})]g\rangle$ have been summed up.

$$\frac{\sigma(e^+e^- \to \gamma^* \to |(c\bar{c})[(1^3S_1^{(\mathbf{8})})]g\rangle + c\bar{c} \to J/\psi + c\bar{c})}{\sigma(e^+e^- \to \gamma^* \to |(c\bar{c})[(1^3S_1^{(\mathbf{1})})]\rangle + c\bar{c} \to J/\psi + c\bar{c})} \sim 3.1\%,$$

$$\frac{\sigma(e^+e^- \to \gamma^* \to |(c\bar{c})[(1^3S_1^{(\mathbf{8})})]g\rangle + c\bar{c} \to \chi_{cJ} + c\bar{c})}{\sigma(e^+e^- \to \gamma^* \to |(c\bar{c})[(1^3P_J^{(\mathbf{1})})]\rangle + c\bar{c} \to \chi_{cJ} + c\bar{c})} \sim 19\%.$$

- At the super Z factory, it is noted that the channel $e^+e^- \to Z^0 \to |(Q\bar{Q})[(1^1S_0^{(\mathbf{8})}), (1^3S_1^{(\mathbf{8})})]g\rangle + g$ is less important than the case of $e^+e^- \to Z^0 \to |(Q\bar{Q})[(1^1S_0^{(\mathbf{8})}), (1^3S_1^{(\mathbf{8})})]g\rangle + Q\bar{Q}$ by at least an order of magnitude for the production of ψ_Q, h_Q and χ_{QJ}. While at the B factory, the channel $e^+e^- \to \gamma^* \to |(Q\bar{Q})[1^1S_0^{(\mathbf{8})}]g\rangle + g$ is significant,

$$\frac{\sigma(e^+e^- \to \gamma^* \to |(c\bar{c})[(1^1S_0^{(\mathbf{8})})]g\rangle + g \to J/\psi + g)}{\sigma(e^+e^- \to \gamma^* \to |(c\bar{c})[(1^3S_1^{(\mathbf{1})})]\rangle + c\bar{c} \to J/\psi + c\bar{c})} \sim 30\%.$$

2. *Differential cross sections for the octet channels*

To show the relative importance among different channels as indicated by Tables XII and XIII more clearly, we present the P_t and rapidity $y-$ distributions for the octet production channels of J/ψ, Υ, h_c, h_b, χ_{cJ} and χ_{bJ} in Figs.(15,16). Furthermore, the total cross sections with different p_{tcut} and y_{cut} are presented in Tables XIV and XV. They show that the channel $e^+e^- \to Z^0 \to |(Q\bar{Q})[(1^3S_1^{(\mathbf{8})})]g\rangle + Q\bar{Q}$ will lead to a peak in low P_t region, about 5 GeV for charmonium and 10 GeV for bottomonium.

As a final remark, to be useful reference, we present the charmonium and bottomonium P_t distribution with various rapidity cut (y_{cut}) and their y distributions with various transverse momentum cut (P_{tcut}) for the channel $e^+e^- \to Z^0 \to |H_Q\rangle + Q\bar{Q}$ in Figs.(17,18,19,20). In these figures, both color-singlet and color-octet contributions are taken into consideration. Here, for the ψ_Q production through $e^+e^- \to Z^0 \to \psi_Q + Q\bar{Q}$, the components $|(Q\bar{Q})[\left(1^1S_0^{(\mathbf{8})}\right)]g\rangle, |(Q\bar{Q})[\left(1^3S_1^{(\mathbf{8})}\right)]g\rangle$ and $|(Q\bar{Q})[\left(1^3S_1^{(\mathbf{1})}\right)]\rangle$ have been summed up. While, for the P-wave quarkonium production through $e^+e^- \to Z^0 \to (h_Q, \chi_{QJ}) + Q\bar{Q}$, the contributions to h_Q and χ_{QJ} production, including both color-singlet and color-octet contributions, have been summed up.

IV. SUMMARY

In this paper, we have studied the charmonium and bottomonium production through the e^+e^- annihilation in the leading α_s-order. A detailed discussion on the heavy quarkonium production at the super Z factory via the two types of semi-exclusive channels, $e^+e^- \to |H_{Q\bar{Q}}\rangle + X$ with $X = Q\bar{Q}$ or gg, have been presented.

As usual, total cross sections are dominated by the color-singlet $1S$-level quarkonium states. However the color-singlet quarkonium states at the $2S$-level and the $1P$-level, and the color-octet quarkonium state $|(Q\bar{Q})[1^3S_1^{(\mathbf{8})}]g\rangle$ can also provide sizable contributions. Total cross sections for the color-singlet channels versus the collision energy E_{cm} have been presented in Figs.(6,7,8,9). The curves for the color-octet S-wave states have the same shapes with the corresponding color-singlet S-wave states. In the low collision energy region, the cross sections are dominated by the processes via the γ^* propagator (agree with observation at the B factory): main contributions are around $6-20$ GeV for charmonium production and $10-40$ GeV for bottomonium production. Around the collision energy $E_{cm} = m_Z$, due to the Z^0-boson resonance effect, the cross sections become much larger for the processes via the Z^0 propagator. Then, in even higher energies, the total cross section drops down logarithmically for all the processes. By varying E_{cm} within the range of $(1 \pm 3\%)m_Z$, the total cross sections changes down to $\binom{18\%}{17\%}$ of its peak value for $e^+e^- \to Z^0 \to J/\psi + c\bar{c}$, which is down to $\binom{18\%}{16\%}$ for $e^+e^- \to Z^0 \to \Upsilon + b\bar{b}$.

At the super Z factory, the heavy quarkonium production processes $e^+e^- \to |H_{Q\bar{Q}}\rangle + X$ are dominated by those via the Z^0 propagator. Comparing to their productions at the B factories (running at the energy scale around 10.6 GeV), total cross sections of $e^+e^- \to |H_{Q\bar{Q}}\rangle + X$ become much larger in the super Z-factory or the GigaZ program of ILC. A programming high luminosity of the super Z factory is also helpful for accumulating data. For example, we estimate the number of events under the luminosity $\mathcal{L} = 10^{34}\mathrm{cm}^{-2}\mathrm{s}^{-1}(\simeq 10^5\mathrm{pb}^{-1}/\mathrm{year}$ [56]). Setting N_H to stand for the number of hadron H events generated per year, for the charmonium production, we obtain

$$\begin{aligned} N_{J/\psi} &= 2.74\times 10^5\,, N_{\psi'} = 1.16\times 10^5\,, N_{\eta_c} = 1.76\times 10^5, \\ N_{\eta_c'} &= 1.11\times 10^5\,, N_{h_c} = 2.41\times 10^4\,, N_{\chi_{c0}} = 7.37\times 10^4, \\ N_{\chi_{c1}} &= 1.55\times 10^5\,, N_{\chi_{c2}} = 2.17\times 10^5 \end{aligned}$$

for the process $e^+e^- \to |H_{c\bar{c}}\rangle + c\bar{c}$;

$$\begin{aligned} N_{J/\psi} &= 3.91\times 10^3\,, N_{\psi'} = 2.47\times 10^3\,,\ N_{\eta_c} = 1.72\times 10^4, \\ N_{\eta_c'} &= 1.09\times 10^4 \end{aligned}$$

for the process $e^+e^- \to |H_{c\bar{c}}\rangle + gg$. For the bottomonium production, we obtain

$$\begin{aligned} N_{\Upsilon} &= 2.22\times 10^4\,, N_{\Upsilon'} = 1.08\times 10^4\,, N_{\eta_b} = 1.94\times 10^4, \\ N_{\eta_b'} &= 9.60\times 10^3\,, N_{h_b} = 7.22\times 10^2\,, N_{\chi_{b0}} = 1.58\times 10^3, \\ N_{\chi_{b1}} &= 2.52\times 10^3\,, N_{\chi_{b2}} = 2.90\times 10^2 \end{aligned}$$

for the process $e^+e^- \to |H_{b\bar{b}}\rangle + b\bar{b}$;

$$\begin{aligned} N_{\Upsilon} &= 6.55\times 10^3\,, N_{\Upsilon'} = 3.24\times 10^3\,, N_{\eta_b} = 8.18\times 10^3, \\ N_{\eta_b'} &= 4.05\times 10^3 \end{aligned}$$

for the process $e^+e^- \to |H_{b\bar{b}}\rangle + gg$. Thus, in addition to the B-factories as BABAR and Belle and the hadronic colliders as Tevatron and LHC, the super Z-factory will provide an excellent platform for studying the heavy quarkonium properties.

For the charmonium or bottomonium production channels via the Z^0 propagator, there is approximate "spin degeneracy". Taking the charmonium production channels as an example, we obtain

$$\frac{\sigma_{e^+e^-\to Z^0\to\eta_c+c\bar{c}}}{\sigma_{e^+e^-\to Z^0\to J/\psi+c\bar{c}}} \simeq 96\%$$

and

$$\frac{\sigma_{e^+e^-\to Z^0\to\chi_{c0}+c\bar{c}}}{\sigma_{e^+e^-\to Z^0\to\chi_{c1}+c\bar{c}}} \simeq 91\%.$$

Such "spin degeneracy" is confirmed by analyzing the quarkonium p_t- and y- distributions, and also by a cross check from the fragmentation approach.

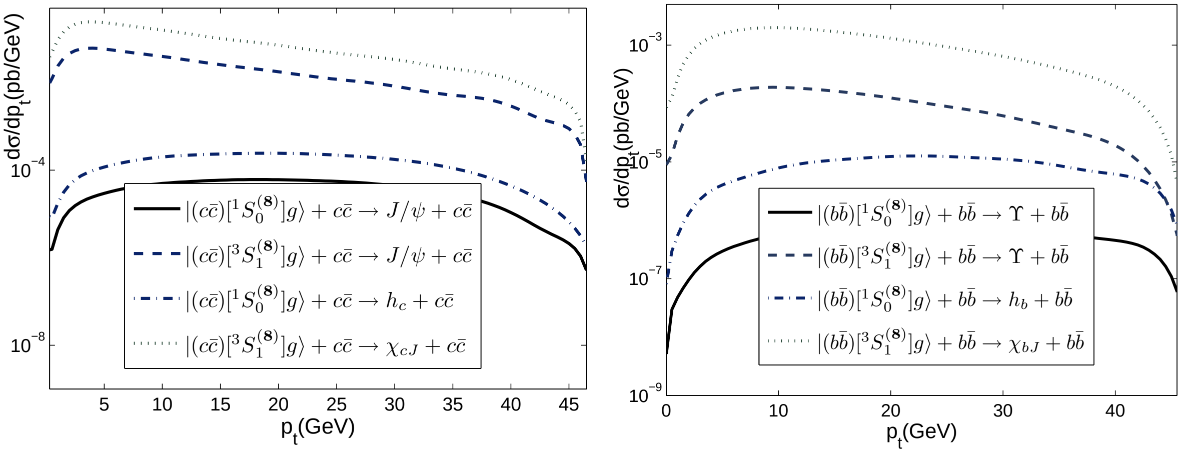

FIG. 15: The charmonium (Left) and bottomonium (Right) P_t-distributions via the production processes, $e^+e^- \to Z^0 \to |(Q\bar{Q})[\left(1^1S_0^{(\mathbf{8})}\right), \left(1^3S_1^{(\mathbf{8})}\right)]g\rangle + Q\bar{Q} \to (\psi_Q, h_Q, \chi_{QJ}) + Q\bar{Q}$. The collision energy $E_{cm} = m_Z$.

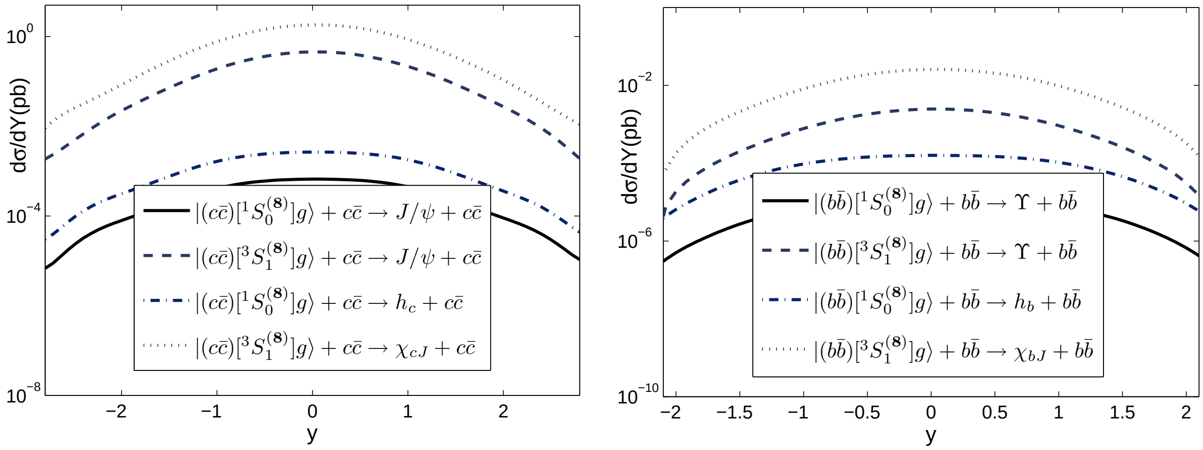

FIG. 16: The charmonium (Left) and bottomonium (Right) y-distributions via the production processes, $e^+e^- \to Z^0 \to |(Q\bar{Q})[\left(1^1S_0^{(\mathbf{8})}\right), \left(1^3S_1^{(\mathbf{8})}\right)]g\rangle + Q\bar{Q} \to (\psi_Q, h_Q, \chi_{QJ}) + Q\bar{Q}$. The collision energy $E_{cm} = m_Z$.

We have also discussed the uncertainties caused by the effective quark masses. For the charmonium production channel $e^+e^- \to Z^0 \to |H_{c\bar{c}}\rangle + X$, when $X = c\bar{c}$, the uncertainties caused by varying $m_c = 1.50 \pm 0.15$ GeV are $\sim 40\%$ for the S-wave case, which change to be $\sim 70\%$ for the P-wave case; when $X = gg$, the uncertainties for both the S-wave and P-wave cases are $\sim 15\% - 19\%$. For the bottominum production channel $e^+e^- \to Z^0 \to |H_{b\bar{b}}\rangle + X$, when $X = b\bar{b}$, the uncertainties caused by varying $m_b = 4.90 \pm 0.15$ GeV are $\sim 11\%$ for the S-wave case, which change to be $\sim 15\% - 18\%$ for the P-wave case; when $X = gg$, the uncertainties for both the S-wave and P-wave cases are $\sim 6\%$. To depress the theoretical uncertainty at such a super Z factory, it is helpful to finish a next-to-leading order calculation for the channel $e^+e^- \to Z^0 \to |H_{c\bar{c}}\rangle + X$, which is in progress.

V. ACKNOWLEDGMENTS

This work was supported in part by the Fundamental Research Funds for the Central Universities under Grant No. CDJXS12300004 and CQDXWL-2012-Z002, the Program for New Century Excellent Talents in University under Grant No. NCET-10-0882, and the Natural Science Foundation of China under Grant No. 11075225 and No. 11275280.

P_{tcut}(GeV)	5	10	15
$\sigma(e^+e^- \to Z^0 \to \vert(c\bar{c})[(1^1S_0^{(\mathbf{8})})]g\rangle + c\bar{c} \to J/\psi + c\bar{c})$	1.62×10^{-3}(96%)	1.41×10^{-3}(83%)	1.13×10^{-3}(67%)
$\sigma(e^+e^- \to Z^0 \to \vert(c\bar{c})[(1^3S_1^{(\mathbf{8})})]g\rangle + c\bar{c} \to J/\psi + c\bar{c})$	6.80×10^{-1}(75%)	4.41×10^{-1}(48%)	2.85×10^{-1}(31%)
$\sigma(e^+e^- \to Z^0 \to \vert(c\bar{c})[(1^1S_0^{(\mathbf{8})})]g\rangle + c\bar{c} \to h_c + c\bar{c})$	6.50×10^{-3}(96%)	5.65×10^{-3}(83%)	4.54×10^{-3}(67%)
$\sigma(e^+e^- \to Z^0 \to \vert(c\bar{c})[(1^3S_1^{(\mathbf{8})})]g\rangle + c\bar{c} \to \chi_{cJ} + c\bar{c})$	2.72(75%)	1.76(48%)	1.14(31%)
$\sigma(e^+e^- \to Z^0 \to \vert(b\bar{b})[(1^1S_0^{(\mathbf{8})})]g\rangle + b\bar{b} \to \Upsilon + b\bar{b})$	2.69×10^{-5}(97%)	2.46×10^{-5}(89%)	2.11×10^{-5}(76%)
$\sigma(e^+e^- \to Z^0 \to \vert(b\bar{b})[(1^3S_1^{(\mathbf{8})})]g\rangle + b\bar{b} \to \Upsilon + b\bar{b})$	3.80×10^{-3}(90%)	2.90×10^{-3}(69%)	2.02×10^{-3}(48%)
$\sigma(e^+e^- \to Z^0 \to \vert(b\bar{b})[(1^1S_0^{(\mathbf{8})})]g\rangle + b\bar{b} \to h_b + b\bar{b})$	3.66×10^{-4}(97%)	3.34×10^{-4}(89%)	2.87×10^{-4}(76%)
$\sigma(e^+e^- \to Z^0 \to \vert(b\bar{b})[(1^3S_1^{(\mathbf{8})})]g\rangle + b\bar{b} \to \chi_{bJ} + b\bar{b})$	3.99×10^{-2}(90%)	3.05×10^{-2}(69%)	2.12×10^{-2}(48%)

TABLE XIV: Total cross sections (in unit: pb) for the octet-channels of charmonium and bottomonium production via Z^0 propagator at the super Z factory with different P_{tcut}. m_c=1.5 GeV and m_b=4.9 GeV. Here the percentages in the parentheses represent the ratios between the cross sections with various P_{tcut} and the one without P_t cut.

y_{cut}	0.5	1.0	1.5
$\sigma(e^+e^- \to Z^0 \to \vert(c\bar{c})[(1^1S_0^{(\mathbf{8})})]g\rangle + c\bar{c} \to J/\psi + c\bar{c})$	6.45×10^{-4}(38%)	1.18×10^{-3}(70%)	1.49×10^{-3}(88%)
$\sigma(e^+e^- \to Z^0 \to \vert(c\bar{c})[(1^3S_1^{(\mathbf{8})})]g\rangle + c\bar{c} \to J/\psi + c\bar{c})$	4.26×10^{-1}(47%)	7.14×10^{-1}(78%)	8.48×10^{-1}(93%)
$\sigma(e^+e^- \to Z^0 \to \vert(c\bar{c})[(1^1S_0^{(\mathbf{8})})]g\rangle + c\bar{c} \to h_c + c\bar{c})$	2.59×10^{-3}(38%)	4.73×10^{-3}(70%)	5.98×10^{-3}(88%)
$\sigma(e^+e^- \to Z^0 \to \vert(c\bar{c})[(1^3S_1^{(\mathbf{8})})]g\rangle + c\bar{c} \to \chi_{cJ} + c\bar{c})$	1.71(47%)	2.86(78%)	3.40(93%)
$\sigma(e^+e^- \to Z^0 \to \vert(b\bar{b})[(1^1S_0^{(\mathbf{8})})]g\rangle + b\bar{b} \to \Upsilon + b\bar{b})$	1.14×10^{-5}(41%)	2.07×10^{-5}(75%)	2.58×10^{-5}(93%)
$\sigma(e^+e^- \to Z^0 \to \vert(b\bar{b})[(1^3S_1^{(\mathbf{8})})]g\rangle + b\bar{b} \to \Upsilon + b\bar{b})$	2.27×10^{-3}(54%)	3.63×10^{-3}(86%)	4.13×10^{-3}(98%)
$\sigma(e^+e^- \to Z^0 \to \vert(b\bar{b})[(1^1S_0^{(\mathbf{8})})]g\rangle + b\bar{b} \to h_b + b\bar{b})$	1.55×10^{-4}(41%)	2.81×10^{-4}(75%)	3.51×10^{-4}(93%)
$\sigma(e^+e^- \to Z^0 \to \vert(b\bar{b})[(1^3S_1^{(\mathbf{8})})]g\rangle + b\bar{b} \to \chi_{bJ} + b\bar{b})$	2.38×10^{-2}(54%)	3.81×10^{-2}(86%)	4.33×10^{-2}(98%)

TABLE XV: Total cross sections (in unit: pb) for the octet-channels of charmonium and bottomonium production via Z^0 propagator at the super Z factory with different y_{cut}. m_c=1.5 GeV and m_b=4.9 GeV. Here the percentages in the parentheses represent the ratios between the cross sections with various y_{cut} and the one without rapidity cut.

Appendix A: Phase space splitting for the color-singlet case

Generally, we can factorize the $2 \to 3$ phase phase into two parts

$$\begin{aligned}
&\mathrm{d}\Phi_3(p_1+p_2;p_3,p_4,p_5)\\
&= (2\pi)^4\delta^{(4)}\left(p_1+p_2-\sum_{i=3}^{5}p_i\right)\prod_{j=3}^{5}\frac{\mathrm{d}^3p_j}{(2\pi)^3 2E_j}\\
&= \mathrm{d}\Phi_2(q;p_1,p_2)\frac{\mathrm{d}q^2}{2\pi}\mathrm{d}\Phi_3(q;p_3,p_4,p_5), \qquad \text{(A1)}
\end{aligned}$$

where $q^2 = (\sum_{i=3}^5 E_i)^2 - |\sum_{i=3}^5 \vec{p}_i|^2$ for $p_i = (E_i, \vec{p}_i)$. At the same time, the hard scattering amplitude can be rewritten as

$$\begin{aligned}
&|\mathcal{M}_{2\to3}|^2\\
&= \left|\mathcal{M}^{\mu}_{2\to1}\left(-g_{\mu\nu}+\frac{q_\mu q_\nu}{M_Z^2}\right)\mathcal{M}^{\nu}_{1\to3}\right|^2\\
&= \left|\sum_{\lambda}\mathcal{M}^{\mu}_{2\to1}\mathcal{M}^{\nu}_{1\to3}\epsilon^*_\mu(q,\lambda)\epsilon_\nu(q,\lambda)\right|^2\\
&= \frac{1}{3}\sum_{\lambda_1,\lambda_2}\left|\mathcal{M}^{\mu}_{2\to1}\epsilon^*_\mu(q,\lambda_1)\right|^2\left|\mathcal{M}^{\nu}_{1\to3}\epsilon_\nu(q,\lambda_2)\right|^2, \text{(A2)}
\end{aligned}$$

where $\epsilon(q,\lambda)$ stands for the Z^0 polarization vector. Then the process $e^+e^- \to |H_{cc}\rangle + c\bar{c}$ can be divided into two parts: the $2 \to 1$ process ($e^+e^- \to Z^0$) and the $1 \to 3$ process ($Z^0 \to |H_{Q\bar{Q}}\rangle + Q\bar{Q}$). The phase space of $2 \to 1$ process can be done easily. And the $1 \to 3$ process is the same as Z^0 decays to three final particles.

---

[1] J.J. Aubert et al., Phys. Rev. Lett. **33**, 1404 (1974); J.E. Augustin et al., Phys. Rev. Lett. **33**, 1406 (1974).

[2] C.H. Chang, Nucl. Phys. B**172**, 425 (1980)

[3] T. Appelquist and H.D. Politzer, Phys. Rev. Lett. **34**, 43 (1975); A. De Rujula and S.L. Glashow, Phys. Rev. Lett. **34**, 46 (1975); C.A. Dominguez and M. Greco, Lett. Nuovo Cim. **12**, 439 (1975).

[4] J.H. Kuhn, J. Kaplan, E.G.O. Safiani, Nucl. Phys. B **157**, 125 (1979); W.Y. Keung, Phys. Rev. D **23**, 2072 (1981); J.H. Kuhn, H. Schneider, Phys. Rev. D **24**, 2996 (1981);

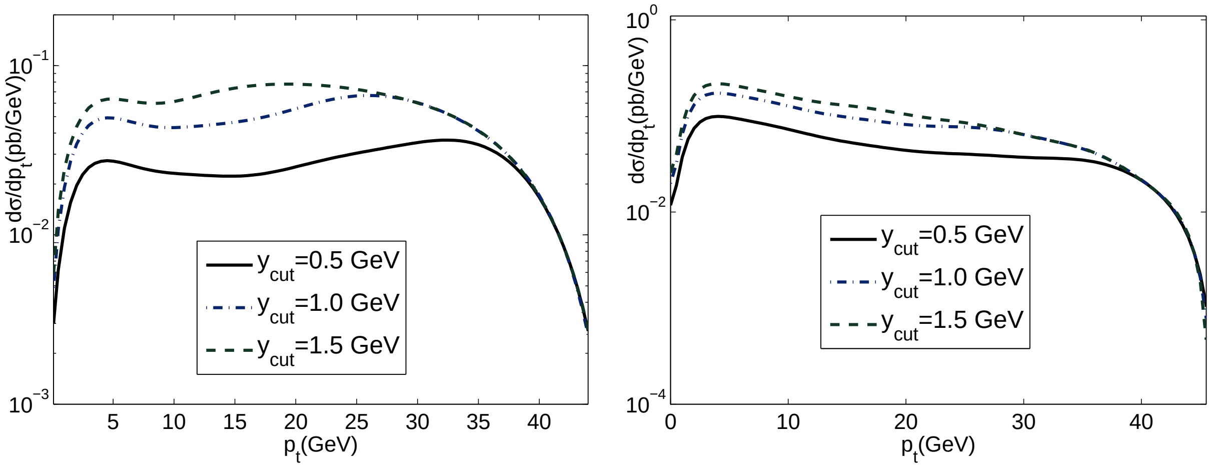

FIG. 17: The charmonium P_t distributions (Left is for J/ψ and Right is for P-wave charmonium) with various y_{cut} for $E_{cm} = m_Z$. $m_c = 1.5$ GeV.

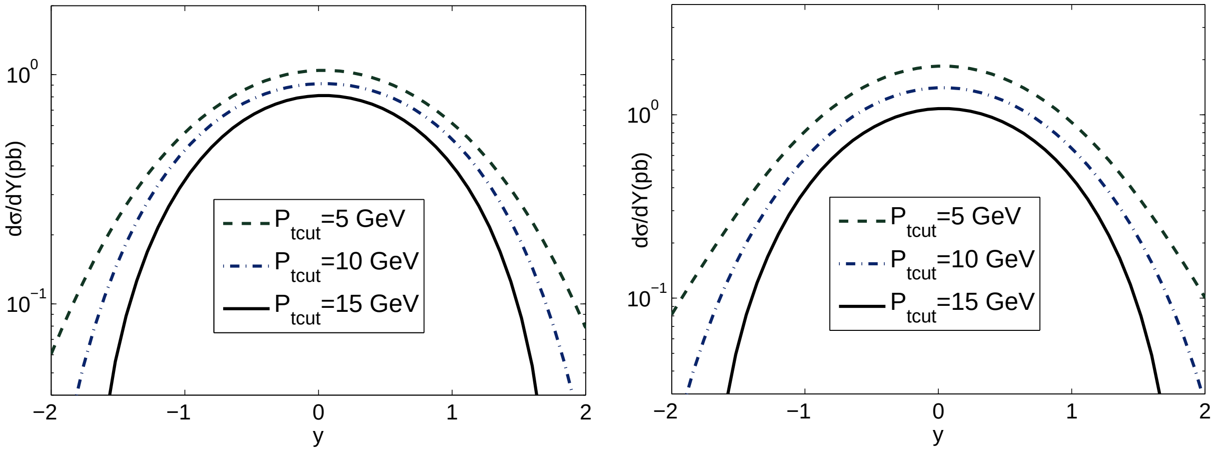

FIG. 18: The charmonium y distributions (Left is for J/ψ and Right is for P-wave charmonium) with various P_{tcut} for $E_{cm} = m_Z$. $m_c = 1.5$ GeV.

J.H. Kuhn, H. Schneider, Z. Phys. C **11**, 263 (1981); L. Clavelli, Phys. Rev. D **26**, 1610 (1982).

[5] K. Hagiwara, A.D. Martin, W.J. Stirling, Phys. Lett. B **267**, 527 (1991); V.M. Driesen, J.H. Kuhn, E. Mirkes, Phys. Rev. D **49**, 3197 (1994).

[6] V.V. Kiselev, A.K. Likhoded, M.V. Shevlyagin, Phys. Lett. B **332**, 411 (1994).

[7] P.L. Cho, A.K. Leibovich, Phys. Rev. D **54**, 6690 (1996).

[8] E. Braaten, Y.Q. Chen, Phys. Rev. Lett. **76**, 730 (1996) .

[9] F. Yuan, C.F. Qiao, K.T. Chao, Phys. Rev. D **56**, 321 (1997).

[10] C.H. Chang, C.F. Qiao, J.X. Wang, Phys. Rev. D **57**, 4035 (1998).

[11] K.Y. Liu, Z.G. He, K.T. Chao, Phys. Rev. D **69**, 094027 (2004).

[12] N. Brambilla, *et al.*, Quarkonium Working Group, arXiv: 0412158; Eur. Phys. J. C **71**, 1534 (2011).

[13] G. Aarons et al. (ILC Collaboration), International Linear Collider Reference Design Report 2 Physics at the ILC (2007).

[14] J. Erler S. Heinemeyerb, W. Hollikc, G. Weigleind, P.M. Zerwasb, Phys. Lett. B **486**, 125 (2000).

[15] J.P. Ma and Z.X. Zhang (The super Z-factory group), Sci. China: Phys., Mech. Astron. **53**, 1947 (2010).

[16] G.T. Bodwin, E. Braaten and G.P. Lepage, Phys. Rev. D **51**, 1125 (1995).

[17] E. Braaten and S. Fleming, Phys. Rev. Lett. **74**, 3327 (1995); M. Cacciari, M. Greco, M.L. Mangano and A. Petrelli, Phys. Lett. B **356**, 553 (1995); E. Braaten and T.C. Yuan, Phys. Rev. D **52**, 6627 (1995).

[18] M. Cacciari and M. Kramer, Phys. Rev. Lett. **76**, 4128 (1996).

[19] M. Beneke and I.Z. Rothstein, Phys. Rev. D **54**, 2005 (1996).

[20] M. Beneke and M. Kramer, Report No. CERN-TH/96-310.

[21] M. A. Sanchis-Lozano and B. Cano-Coloma, Nucl. Phys. Proc. Suppl. **55**A, 277 (1997).

[22] X.G. Wu, C.H. Chang, Y.Q. Chen, Z.Y. Fang, Phys. Rev.

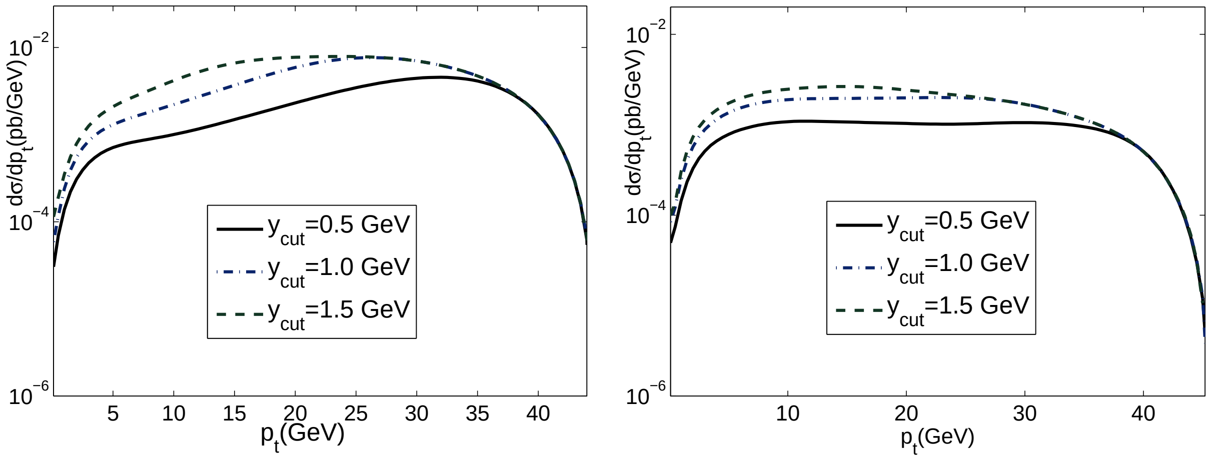

FIG. 19: The bottomonium P_t distributions (Left is for Υ and Right is for P-wave bottomonium) with various y_{cut} for $E_{cm} = m_Z$. $m_b = 4.9$ GeV.

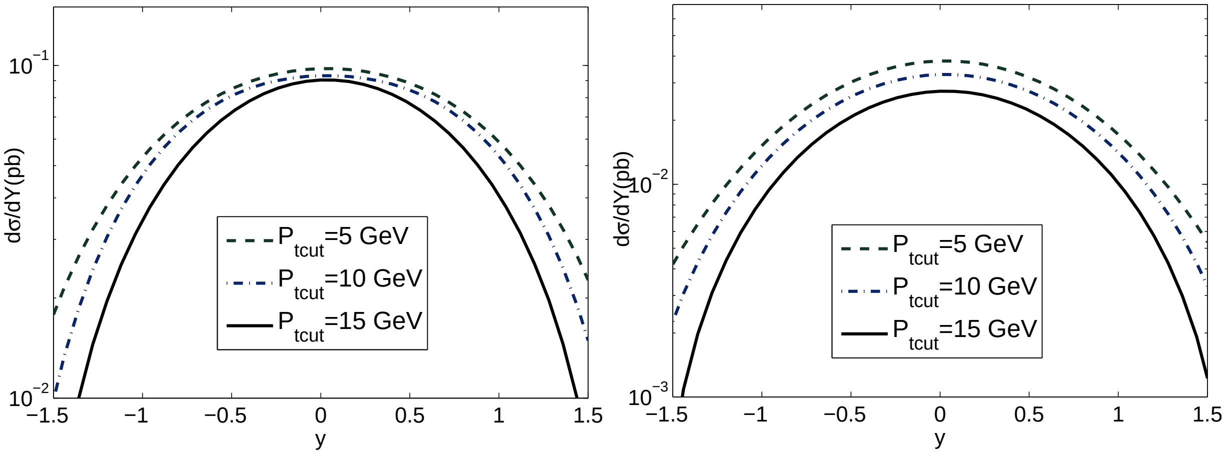

FIG. 20: The bottomonium y distributions (Left is for Υ and Right is for P-wave bottomonium) with various P_{tcut} for $E_{cm} = m_Z$. $m_b = 4.9$ GeV.

D**67**, 094001 (2003).

[23] Y.J. Zhang, Y.Q. Ma, K. Wang and K.T. Chao, Phys. Rev. D**81**, 034015 (2010).

[24] Y.Q. Ma, K. Wang and K.T. Chao, Phys. Rev. Lett. **106**, 042002 (2011).

[25] M. Butenschoen and B.A. Kniehl, Phys. Rev. Lett. **106**, 022003 (2011).

[26] K. Cheung, W.Y. Keung, T.C. Yuan, Phys. Rev. Lett. **76**, 877 (1996).

[27] L.C. Deng, X.G. Wu, Z. Yang, Z.Y. Fang and Q.L. Liao, Eur. Phys. J. C**70**, 113 (2010).

[28] Z. Yang, X.G. Wu, L.C. Deng, J.W. Zhang and G. Chen, Eur. Phys. J. C**71**, 1563 (2011).

[29] C.F. Qiao, L.P. Sun and R.L. Zhu, JHEP **1108**, 131 (2011).

[30] Z. Yang, X.G. Wu, G. Chen, Q.L. Liao and J.W. Zhang, Phys. Rev. D**85**, 094015 (2012).

[31] C.H. Chang, J.X. Wang and X.G. Wu, Sci. China: Phys., Mech. Astron. **53**, 2031 (2010); arXiv:1005.4723.

[32] J. Jiang, X.G. Wu, Q.L. Liao, X.C. Zheng and Z.Y. Fang, Phys. Rev. D **86**, 054021 (2012).

[33] A. Petrelli, M. Cacciari, M. Greco, F. Maltoni, M.L. Mangano, Nucl. Phys. B **514**, 245 (1998).

[34] R. Kleiss and W. J. Stirling, Comput. Phys. Commun. **40**, 359 (1986).

[35] G.P. Lepage, J. Comput. Phys. **27**, 192 (1978).

[36] C.H. Chang, J.X. Wang and X.G. Wu, Comput. Phys. Commun.**177**, 467 (2007); C.H. Chang, J.X. Wang and X.G. Wu, Comput. Phys. Commun.**181**, 1144 (2010); X.Y. Wang and X.G. Wu, Comput. Phys. Commun. **184**, 1070 (2013).

[37] C.H. Chang, C. Driouich, P. Eerola, and X.G. Wu, Comput. Phys. Commun. **159**, 192 (2004); C.H. Chang, J.X. Wang, and X.G. Wu, Comput. Phys. Commun. **174**, 241 (2006); 175, 624 (2006); X.Y. Wang and X.G. Wu, Comput. Phys. Commun. **183**, 442 (2012).

[38] P. Cho, A.K. Leibovich, Phys. Rev. D **53**, 150 (1996); P. Cho, A.K. Leibovich, Phys. Rev. D **53**, 6203 (1996).

[39] J. Beringer *et al.*, (Particle Data Group), Phys. Rev. D**86**, 010001 (2012).

[40] J.D. Bjorken, Phys. Rev. D **17**, 171 (1978).

[41] M. Suzuki, Phys. Lett. B **71**, 139 (1977).

[42] S.J. Brodsky, C. Peterson, and N. Sakai, Phys. Rev. D **23**, 2745 (1981).

[43] C. Peterson, D. Schlatter, I. Schmit, and P.M. Zerwas, Phys. Rev. D **27**, 105 (1983).

[44] L. Clavelli, Phys. Rev. D **26**, 1610 (1982).

[45] C.R. Ji and F. Amiri, Phys. Rev. D **35**, 3318 (1987).

[46] C.R. Ji and F. Amiri, Phys. Lett. B **195**, 593 (1987).

[47] E. Braaten, T.C. Yuan, Phys. Rev. Lett. **71**, 1673 (1993).

[48] C.H. Chang and Y.Q. Chen, Phys. Rev. D **46**, 3845 (1992).

[49] E. Braaten, K. Cheung, and T.C. Yuan, Phys. Rev. D **48**, R5049 (1993).

[50] E. Braaten, K. Cheung, and T.C. Yuan, Phys. Rev. D **48**, 4230 (1993).

[51] M. Suzuki, Phys. Rev. D **33**, 676 (1986).

[52] T.C. Yuan, Phys. Rev. D **50**, 5664 (1994).

[53] M. Cacciari, M. Greco and P. Nason, JHEP **9805**, 007 (1998).

[54] M. Cacciari and P. Nason, Phys. Rev. Lett. **89**, 122003 (2002).

[55] S.J. Brodsky, X.G. Wu, Phys. Rev. Lett. **109**, 042002 (2012); S.J. Brodsky, X.G. Wu, Phys. Rev. D**85**, 034038 (2012); S.J. Brodsky, X.G. Wu, Phys. Rev. D**86**, 054018 (2012); S.J. Brodsky and L.D. Giustino, Phys. Rev. D**86**, 085026 (2012); M. Mojaza, S.J. Brodsky, X.G. Wu, arXiv:1212.0049; X.G. Wu, S.J. Brodsky, M. Mojaza, arXiv:1302.0599;

[56] Tao Han, arXiv:0508097 [hep-ph].